hep-th/0609209
SISSA 57/2006/EP

arXiv:hep-th/0609209 v1 28 Sep 2006

Closed Bosonic String Field Theory at Quintic Order: Five-Tachyon Contact Term and Dilaton Theorem

Nicolas Moeller

International School for Advanced Studies (SISSA)
via Beirut 2-4,
34014 Trieste, Italy

E-mail: moeller@sissa.it

Abstract

We solve the geometry of the closed string field theory five-point vertex. Our solution is calculated in terms of quadratic Strebel differentials which are found numerically all over the relevant subspace of the moduli space of spheres with five punctures. Part of the boundary of the reduced moduli space is described in terms of an algebraic curve, while the remaining part has to be evaluated numerically. We use this data to compute the contact term of five tachyons and estimate its uncertainty to be of about 0.1%. To put to a test the theory and the computations done, we calculate the contact term of five dilatons. In agreement with the dilaton theorem, it is found to cancel the term obtained from the tree level Feynman diagrams built with three- and four-vertices. This cancellation, achieved with a precision of about 0.1%, is within the estimated margin error on the contact term and is therefore a very good evidence that our computations are reliable. The techniques and numerical algorithm developed in this paper make it possible to compute the contact amplitude of any five off-shell closed bosonic string states.

Contents

1 Introduction

The object of this paper is the explicit computation of the quintic term of the action of closed bosonic string field theory (CSFT). This action, formally constructed in [1, 2, 3, 4], is nonpolynomial. This is in contrast with Witten's string field theory [5] which is cubic, i.e. Feynman diagrams constructed with three-vertices are enough to cover (exactly once) the whole moduli space of Riemann surfaces with N punctures on the boundary. In CSFT it is not possible to do so, The Feynman diagrams with closed three-vertices do not suffice to construct all spheres with four punctures, one has to introduce, in the action, a contact term of order four in the string field to account for the remaining four-punctured spheres. But this is not yet enough, one has to introduce also a five-vertex because the Feynman diagrams with three- and four-vertices do not cover the whole moduli space of spheres with five punctures. And so on, one must put in the action, contact terms of all orders. In this paper we will discuss only the classical action, but if we were to consider diagrams with loops, we would face a similar problem; namely the vertices of the classical action are not enough to generate all Riemann surfaces of genus one; and so on, one must introduce terms at all genii.

Being able to explicitly compute the whole action would be immensely useful in understanding nonperturbative physics of closed strings. The hot problem that we have in mind is, in particular, to understand if closed bosonic string theory has a stable vacuum, and what would the theory look

like in this vacuum. The approach that we are taking, is by order truncation of the CSFT action, i.e. we truncate it to a polynomial of a given order in the string field. The simplest nontrivial truncation is done by keeping the quadratic and cubic terms only. In [6], Kostelecký and Samuel did precisely that; they then truncated the string field itself by keeping only the tachyon and all the massless fields. In this approximation they found a locally stable vacuum in which the tachyon had a positive expectation value.

The next order of approximation is to keep the quartic term as well. The computation of this term is already seriously complicated. The reason lies in the fact that, in order to compute a contact amplitude with N external states, one has to integrate a certain correlator over a region of the moduli space of spheres with N punctures (we call this region the *reduced* moduli space, it corresponds to all spheres that cannot be constructed with Feynman diagrams), which has real dimensionality $2(N-3)$. The expression of the correlator at a point in the reduced moduli space, depends on the geometry of the vertex at this point, which in turn is given by the solution of a minimal area problem [4]. For the cubic vertex $N=3$, there is no moduli space to integrate over and it is thus easy to calculate. But for the quartic vertex, there is a two-dimensional reduced moduli space. This vertex was solved numerically in [7]. The solution given there consisted of the boundary of the reduced moduli space in the complex plane, and everywhere in this region the geometry of the vertex was expressed with a quadratic differential (see [8, 9] for details on quadratic differentials) given in terms of a complex parameter $a(\xi,\bar{\xi})$ depending on the coordinates on the reduced moduli space. The solution was explicitly given by a reasonably short fit that can be copied from the paper and used to compute amplitudes with an accuracy of about 0.1%.

The results of [7] were checked by Yang and Zwiebach in [10, 11]. For this, they verified that the quartic term in the effective potential of some marginal fields is seen to vanish as one increases the truncation level of the string field. A similar analysis was made for the effective potential of the dilaton. In particular, they found that the contact quartic term cancels the terms from cubic vertices with a precision of about 0.2%.

In [12, 13], Yang and Zwiebach went on to address the question raised before, whether closed bosonic string theory has a stable vacuum. They started by realizing that the tachyon condensate *must* drive the zero-momentum ghost dilaton. Indeed this state with a peculiar ghost structure, given by

$$|D\rangle = (c_1 c_{-1} - \bar{c}_1 \bar{c}_{-1})\,|0\rangle \tag{1.1}$$

has to be included in the condensate as soon as one considers the quartic vertex.[1] This stems from the fact that the antighost insertion in the correlator, can make the ghost numbers work so that amplitudes with a single dilaton, for example three tachyons and a dilaton, are nonzero. They truncated the string field to level four, including the tachyon (level zero), the dilaton (level two) and four massive scalar fields at level four. And they found that the closed string field theory potential has a local minimum where both the tachyon and dilaton take positive expectation values. They

[1] Several years before the quartic vertex was solved in [7], Belopolsky [14] managed to calculate the tachyon effective potential to order four and he found that it had no minimum. This result, however, didn't take into account the dilaton. In fact, it is understood now that the tachyon effective potential doesn't make much sense because one cannot integrate out the massless dilaton.

also noticed that the depth of this minimum tended to decrease as the level increases, and they made the proposition that this vacuum should have a vanishing action density. They supported this claim by looking at the low-energy effective action of the tachyon, dilaton and metric. They found that if this action has a stable vacuum, its depth must be zero. Although the numerics to level four seemed to confirm this claim, a recent computation to level ten [15] shows that, at quartic order, the value of the potential at the stable vacuum is actually negative and non-zero. The question now is whether higher order terms in the CSFT action can make the shallowness of the potential go to zero, or if it stays finite.

It is clear at this point that we need the quintic term of the CSFT action. In the present paper we solve numerically the geometry of the quintic vertex. This is again done with quadratic differentials. We present in details the algorithm to solve the Strebel condition and we spend quite some time describing the reduced moduli space of spheres with five punctures. It will turn out that we can split it into 120 regions, and need to describe only one of them, that we call $\mathcal{A}_5$. We undertake the description of the boundary of $\mathcal{A}_5$, and to our pleasant surprise we find that its projection on one of its two complex coordinates (corresponding to the two unfixed punctures in the uniformizer coordinate) can be described algebraically in terms of an algebraic curve, that we will be found from the solution of the class of quadratic differentials with two double zeros. The rest of the boundary will be solved numerically. After this is done, we can integrate correlators over the reduced moduli space. The simplest one is the term with five tachyons. We describe in details how we do this integration and how we estimate the uncertainty in the result.

In order to gain confidence in this result, and à fortiori in the machinery developed and the numerical results produced, we must check our algorithm in some way. For this, we compute the effective potential of the dilaton to order five. As the dilaton theorem claims, this should be identically zero. The term of order five is composed of two terms, namely the contact term that we calculate with our algorithm, and the term from Feynman diagrams with vertices of lower order, that we calculate with the techniques and results of [11, 15]. The cancellation is achieved with an accuracy of about 0.1%, falling well within the 0.5% estimated error on the five-dilaton contact term. We therefore claim that our algorithm and result for the five-tachyon term, are reliable. The computation of terms of higher levels, necessary in order to pursue the study of the nonperturbative vacuum of [12, 15], is now possible and will be done in a future publication [16].

We think it is a good idea to give some orders of magnitude related to the algorithm developed here. Its implementation on a computer is done in the C++ language, and the code is more than 10,000 lines long. The complete and accurate computation of the moduli space and the quadratic differentials inside it, takes several days to compute on a desktop computer and generates about one GByte of data. Once this is done, the accurate computation of an integral takes several hours. Unfortunately, the size of the data makes it impossible for now to express the numerical solution in terms of a reasonably short fit, as we did for the quartic vertex [7].

The paper is structured as follows: We end this section by a short summary on the CSFT action. In Section 2, we construct the quadratic differentials pertinent to the five-point vertex, and we study some of their limiting cases in Section 3. We then describe in Section 4 how to solve the

Strebel condition numerically. The reduced moduli space and the way to compute it are described in Section 5. We can then integrate to obtain the first result, namely the five-tachyon contact term, this is done in Section 6. The reliability check with the computation of the dilaton effective potentials is done in Section 7. We end with some discussions on the present results and prospects in Section 8.

We now summarize the CSFT action and fix our notation. With $\alpha' = 2$, the closed string field theory action is [1, 2]

$$S = -\frac{1}{\kappa^2}\left(\frac{1}{2}\langle\Psi|c_0^- Q_B|\Psi\rangle + \frac{1}{3!}\{\Psi,\Psi,\Psi\} + \frac{1}{4!}\{\Psi,\Psi,\Psi,\Psi\} + \frac{1}{5!}\{\Psi,\Psi,\Psi,\Psi,\Psi\} + \dots\right), \quad (1.2)$$

where $c_0^- = \frac{1}{2}(c_0 - \bar{c}_c)$, Q_B is the BRST charge and $\{\dots\}$, are the multilinear string functions. In this paper we won't need to know much about the string field Ψ, except that when considering tachyon condensation we keep only scalars with zero-momentum. Namely

$$|\Psi\rangle = t\,|T\rangle + d\,|D\rangle + \sum_{i>2}\psi_i\,|\Psi_i\rangle\,, \quad (1.3)$$

where Ψ_i, $i > 2$, are massive scalars, and the first two fields are respectively the tachyon

$$|T\rangle = c_1\bar{c}_1|0\rangle\,, \quad (1.4)$$

and the dilaton (1.1). We will often use the notation $V_{\psi_{i_1}\psi_{i_2}\dots\psi_{i_N}}$ to designate the coefficient of $\psi_{i_1}\psi_{i_2}\dots\psi_{i_N}$ in the potential (and it is understood that $\psi_1 = t$ and $\psi_2 = d$).

In CSFT, we introduce the following geometry on an interacting worldsheet. Every external state spans a semi-infinite cylinder of perimeter 2π, and these cylinders intersect on a prism. The prisms of a contact term must have the characteristic that all their nontrivial closed curves must have length greater or equal to 2π, and all edges must have length $\leq \pi$. It can be shown that all other prisms are obtained from Feynman diagrams with vertices of lower orders. The relevant prism for the five-point contact term was first discussed in [3]. It is shown on Figure 1. It is made

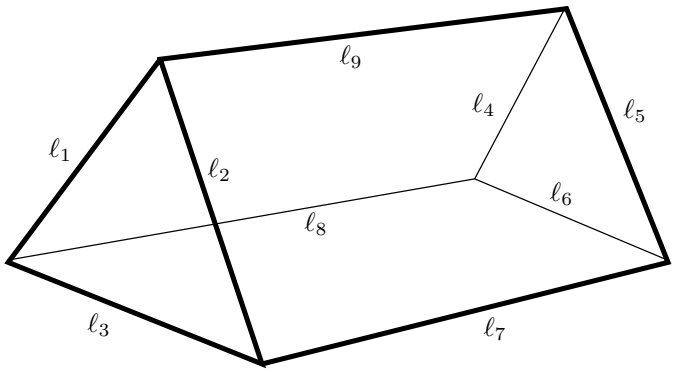

Figure 1: The relevant prism of the five-point vertex. The labeling of lengths will be kept as shown.

of two opposing triangles, connected with three quadrilaterals. The perimeter conditions on the cylinders can be written

$$\begin{aligned} &\ell_1 + \ell_2 + \ell_3 = 2\pi \quad , \quad \ell_4 + \ell_5 + \ell_6 = 2\pi \\ &\ell_7 = \ell_1 + \ell_4 - \pi \quad , \quad \ell_8 = \ell_2 + \ell_5 - \pi \quad , \quad \ell_9 = \ell_3 + \ell_6 - \pi \,. \end{aligned} \tag{1.5}$$

Those are five conditions, leaving four independent lengths, matching the real dimensionality of the moduli space of spheres with five punctures. All other prisms with five faces would have less than four independent lengths and thus correspond to subsets of the moduli space with measure zero. Although they don't contribute to the integration over moduli space, some of these prisms will be considered in Section 3 because they will be useful to calculate the boundaries of the second kind described in Section 5.

The usefulness of this particular geometry is that it arises from a quadratic differential [8] that has second order poles at the punctures where the external states are inserted, and verifies the Strebel condition that its critical graph has measure zero. The ring domains correspond to the semi-infinite cylinders and the critical graph corresponds to the prism.

To be concrete, we will always map the sphere on the complex plane and we will fix the topology of the vertex from the beginning, i.e. we will use the labeling of zeros and poles as indicated on the right of Figure 2. Fixing the topology means that we will only consider configurations obtained from this one by a continuous transformation and without any two zeros merging. In other words, the punctures on quadrilateral faces will always be mapped to $z = 0$, $z = 1$ and $z = \infty$, whereas the remaining punctures at ξ_1 and ξ_2 will always correspond to triangular faces. In these notations, the two complex numbers ξ_1 and ξ_2 parameterize the moduli space of five-punctured spheres.

2 Quadratic differentials

To describe the right geometry and the local coordinates on a punctured sphere, we need a quadratic differential φ, transforming like

$$\varphi = \phi(z)(dz)^2 = \phi(w)(dw)^2 \tag{2.1}$$

under a conformal change of variable. It should be holomorphic everywhere except at the punctures z_I, where it has poles of order two with "residue" minus one, and has thus the expansion

$$\phi(z) = \frac{-1}{(z - z_I)^2} + \mathcal{O}\left((z - z_I)^{-1}\right) \,. \tag{2.2}$$

If we place a puncture at infinity, as we will, the expansion of φ in the coordinate $t = 1/z$ is

$$\phi(t) = \frac{-1}{t^2} + \mathcal{O}\left(t^{-1}\right) \,. \tag{2.3}$$

It is easily seen that the quadratic differentials obeying these conditions are given by

$$\boxed{\phi(z) = -\frac{z^6 + P_5(z) + a_1\, z(z-1)(z-\xi_1)(z-\xi_2) + a_2\, z^2(z-1)(z-\xi_1)(z-\xi_2)}{z^2\,(z-1)^2\,(z-\xi_1)^2\,(z-\xi_2)^2}} \,. \tag{2.4}$$

Here $P_5(z)$ is a polynomial of order five given by (2.12), and a_1 and a_2 do not change the residue conditions at the poles. The coefficient of z^6 in the numerator must be -1 for the residue at infinity to be -1, and we will soon write a solution for $P_5(z)$ that obeys the residue conditions. The parameters a_1 and a_2 will then be determined by the Strebel condition, namely the condition that the critical graph of φ closes (see [8, 9, 14, 7] for more details). It will be enough to know here that the Strebel solution gives the quadratic differential needed for the vertex. It can be expressed as the requirement that the complex lengths between any two zeros z_1 and z_2 of the quadratic differential, are real

$$\mathrm{Im} \int_{z_1}^{z_2} \sqrt{\phi(z)}\, dz = 0\,. \tag{2.5}$$

Solving numerically the Strebel condition will be the object of Section 4. For now let us go back to $P_5(z)$. We will write it in the form

$$P_5(z) = b_5\, z^5 + b_4\, z^4 + P_3(z)\,, \tag{2.6}$$

where

$$P_3(z) = b_3\, z^3 + b_2\, z^2 + b_1\, z + b_0\,. \tag{2.7}$$

The four coefficients of $P_3(z)$ can be completely determined, in terms of ξ_1, ξ_2, b_5 and b_4, by the four residue conditions at the finite poles 0, 1, ξ_1 and ξ_2. These conditions can be written

$$\begin{aligned}
y_0 &\equiv P_3(0) = \xi_1^2\,\xi_2^2 \\
y_1 &\equiv P_3(1) = -1 - b_5 - b_4 + (1-\xi_1)^2(1-\xi_2)^2 \\
y_2 &\equiv P_3(\xi_1) = -\xi_1^6 - b_5\,\xi_1^5 - b_4\,\xi_1^4 + \xi_1^2(\xi_1-1)^2(\xi_1-\xi_2)^2 \\
y_3 &\equiv P_3(\xi_2) = -\xi_2^6 - b_5\,\xi_2^5 - b_4\,\xi_2^4 + \xi_2^2(\xi_2-1)^2(\xi_1-\xi_2)^2\,.
\end{aligned} \tag{2.8}$$

The polynomial P_3 that satisfies (2.8) can be written

$$\begin{aligned}
P_3(z) \;=\; & \frac{(z-1)(z-\xi_1)(z-\xi_2)}{-\xi_1\,\xi_2}\, y_0 + \frac{z(z-\xi_1)(z-\xi_2)}{(1-\xi_1)(1-\xi_2)}\, y_1 + \\
& + \frac{z(z-1)(z-\xi_2)}{\xi_1(\xi_1-1)(\xi_1-\xi_2)}\, y_2 + \frac{z(z-1)(z-\xi_1)}{\xi_2(\xi_2-1)(\xi_2-\xi_1)}\, y_3\,.
\end{aligned} \tag{2.9}$$

Now we want to choose b_5 and b_4 in (2.6) in such a way that the expression (2.9) is as simple as possible. For this we note, from (2.8), that if

$$\begin{aligned}
& b_4 + b_5\,\xi_1 + \xi_1^2 = 0 \\
\text{and} \qquad & b_4 + b_5\,\xi_2 + \xi_2^2 = 0\,,
\end{aligned} \tag{2.10}$$

then the third and fourth terms in (2.9) will be simplified. Even better, since the solution of (2.10) is

$$\begin{aligned}
b_5 &= -(\xi_1 + \xi_2) \\
b_4 &= \xi_1\,\xi_2\,,
\end{aligned} \tag{2.11}$$

we have that $-1-b_5-b_4=-(1-\xi_1)(1-\xi_2)$, and thus we see, from (2.8), that the second term will be simplified too. And obviously, since $y_0=\xi_1^2\xi_2^2$, we also have that the first term is simplified. Thus, making the choice (2.11) for b_5 and b_4, we have that

$$\boxed{P_5(z)=-s\,z^5+t\,z^4+(-s+v(s-1))\,z^3+\left(t+s^2+v(1-s-t)\right)\,z^2+t\,(v-2s)\,z+t^2}\,, \quad (2.12)$$

where

$$\begin{aligned} s &\equiv \xi_1+\xi_2 \\ t &\equiv \xi_1\,\xi_2 \\ v &\equiv (\xi_1-\xi_2)^2=s^2-4t \end{aligned} \quad (2.13)$$

are symmetric expressions in ξ_1 and ξ_2.

We note, for future reference, that the derivatives of $\phi(z)$ with respect to a_1 and a_2 are

$$\begin{aligned} \frac{\partial\phi(z)}{\partial a_1} &= \frac{-1}{z\,(z-1)\,(z-\xi_1)\,(z-\xi_2)}\,, \\ \frac{\partial\phi(z)}{\partial a_2} &= \frac{-1}{(z-1)\,(z-\xi_1)\,(z-\xi_2)}\,. \end{aligned} \quad (2.14)$$

The most uniform prism

We call the *most uniform prism*, the prism (Figure 1) which has two equilateral triangles. The lengths of the edges of the triangles must therefore be $\frac{2\pi}{3}$, and the three edges connecting the two triangles must have lengths $\frac{\pi}{3}$. We want to describe the quadratic differential of this configuration in the z-plane, where we will put three punctures at respectively zero, one and infinity. As already mentioned, we have to start by deciding which faces will correspond to these three punctures. Since we are later going to consider the subgroup of $\mathrm{PSL}(2,\mathbb{C})$ conformal transformations that permute the aforementioned punctures, it will be simplest to map the three quadrilateral faces on $z=0$, $z=1$ and $z=\infty$. We must then stick to this choice because it would be very difficult for the numerical algorithm to switch between configurations of different topologies; this will be discussed more extensively in Section 5. For the purpose of finding the quadratic differential of the most uniform prism, it is easier to work in another coordinate w, where the symmetry of the prism is more visible (see Figure 2). In the w coordinate, $\phi(w)$ has three poles at the vertices of an equilateral triangle, respectively $w=-1$, $w=e^{\frac{i\pi}{3}}$ and $w=e^{-\frac{i\pi}{3}}$, which correspond to the quadrilateral faces. One pole is at its center $w=0$, and the last pole is at infinity. By contemplating the left half of Figure 2, we can immediately write the ansatz for the zeros w_i, $i=1,\ldots,6$, of $\phi(w)$

$$\begin{aligned} &w_1=\beta\,, \quad w_2=e^{\frac{2i\pi}{3}}\beta\,, \quad w_3=e^{\frac{4i\pi}{3}}\beta \\ &w_4=\gamma\,, \quad w_5=e^{\frac{2i\pi}{3}}\gamma\,, \quad w_6=e^{\frac{4i\pi}{3}}\gamma\,, \end{aligned} \quad (2.15)$$

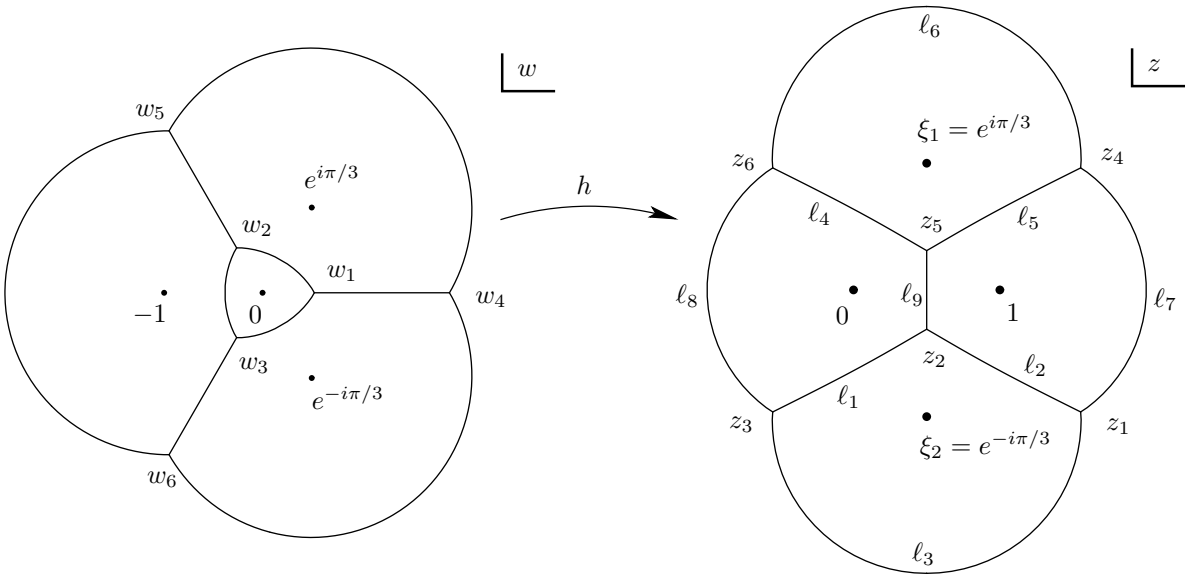

Figure 2: The critical graph of the quadratic differential corresponding to the most uniform prism, in the w-plane where the symmetry is obvious, and in the z-plane in which the three quadrilateral punctures are at the standard points 0, 1, ∞.

where β and γ are positive real numbers and $\gamma > \beta$. The quadratic differential for this configuration is thus

$$\begin{aligned}\phi(w) &= \frac{-(w-\beta)(w-\gamma)(w-e^{\frac{2i\pi}{3}}\beta)(w-e^{\frac{2i\pi}{3}}\gamma)(w-e^{\frac{4i\pi}{3}}\beta)(w-e^{\frac{4i\pi}{3}}\gamma)}{w^2\,(w+1)^2\,\left(w-e^{\frac{i\pi}{3}}\right)^2\,\left(w-e^{-i\frac{\pi}{3}}\right)^2} \\ &= -\frac{\left(w^3-\beta^3\right)\left(w^3-\gamma^3\right)}{w^2\,(w^3+1)^2}\,. \end{aligned} \tag{2.16}$$

The residue condition at $w=-1$ and $w=0$ are respectively

$$\frac{(\beta^3+1)\,(\gamma^3+1)}{9} = 1 \qquad , \qquad \beta^3\,\gamma^3 = 1\,. \tag{2.17}$$

The solution to the system (2.17) with the constraint $\gamma > \beta > 0$ is

$$\beta = \left(\frac{7-3\sqrt{5}}{2}\right)^{\frac{1}{3}} \quad , \quad \gamma = \left(\frac{7+3\sqrt{5}}{2}\right)^{\frac{1}{3}}\,. \tag{2.18}$$

Now we express the quadratic differential in the z coordinate. We want to map the three quadrilateral punctures to $z=0$, $z=1$ and $z=\infty$. Namely $z=h(w)$, where

$$h(-1)=0 \quad , \quad h(e^{\frac{i\pi}{3}})=1 \quad , \quad h(e^{-\frac{i\pi}{3}})=\infty\,, \tag{2.19}$$

whence

$$z = h(w) = e^{\frac{i\pi}{3}}\,\frac{1+w}{w-e^{-\frac{i\pi}{3}}}\,, \tag{2.20}$$

which has the inverse

$$w = h^{-1}(z) = \frac{e^{-\frac{i\pi}{3}} z + e^{\frac{i\pi}{3}}}{z - e^{\frac{i\pi}{3}}} \,. \tag{2.21}$$

Remembering that

$$\phi(z) = \phi(w) \left(\frac{dw}{dz} \right)^2 \,, \tag{2.22}$$

we find

$$\phi(z) = -\frac{z^6 - 3z^5 + 3z^4 - z^3 + 3z^2 - 3z + 1}{z^2(z-1)^2(z-\xi_1)^2(z-\xi_2)^2} \,, \tag{2.23}$$

where the poles ξ_1 and ξ_2 are

$$\begin{aligned} \xi_1 &= h(\infty) = e^{\frac{i\pi}{3}} \\ \xi_2 &= h(0) = e^{-\frac{i\pi}{3}} \,. \end{aligned} \tag{2.24}$$

Now we can easily determine the parameters a_1 and a_2 by comparing (2.4) and (2.12) with (2.23). We find

$$a_1 = a_2 = -2 \,. \tag{2.25}$$

At last, the zeros of $\phi(z)$ are given by

$$z_i = h(w_i) \quad , \quad i = 1, \ldots, 6 \,, \tag{2.26}$$

and their positions are shown on Figure 2. It is important to know an exact quadratic differential for the numerical algorithm to start with. It will then cover all the reduced moduli space by successive deformations of this solution, each deformation being relatively small for the Newton method to converge (more on this in Section 4).

3 Limits of quadratic differentials

One of the most complicated problems in the computation undertaken in this paper, is to describe the boundary of the reduced moduli space. As was already noted in [3], there are two kinds of boundaries. When the length of one of the triangle edges is π, we are on a boundary of the first kind, corresponding to the situation in which the vertex can be built as a Feynman diagram with a propagator of zero length. There are also boundaries of the second kind, when one of the lengths ℓ_7, ℓ_8 or ℓ_9 is zero. These are internal boundaries, they connect prisms with different assignations of punctures to faces. They are not boundaries of the whole reduced moduli space, but they are boundaries of the region $\mathcal{A}_5$ that we will consider by keeping a fixed assignment of punctures to faces (see Section 5). We will also need to consider intersections of boundaries, in particular when two edges have vanishing lengths. The description of the moduli space will be done in Section 5. The problem for now is that when a length vanishes, the quadratic differential has a double zero and it becomes numerically ill-conditioned. The goal of this section is precisely to deal with these limit cases. We can get rid of the numerical difficulties by some analytical work. Actually in the case of two double zeros, the Strebel differentials can be explicitly described in terms of an algebraic curve, reducing the numerical work to finding the roots of a polynomial of order six.

3.1 Quadratic differentials with one double zero

The general case

When we compute the boundary of the reduced moduli space, we are led to consider configurations where the quadratic differential has a double zero, or in other words when an edge collapses to zero length. We have to distinguish whether the collapsed edge is an edge of a triangle or one of the three edges connecting the two triangles. In the first case we end up with a face with only two edges, and for this configuration to be in the reduced moduli space, they need to have length π. The remaining six lengths are constrained by four residue conditions, and we are therefore left with two real degrees of freedom. In the second case, we have eight lengths constrained by five residue conditions, which leave us three degrees of freedom. We are thus going to consider this case only as this will describe some boundaries of the reduced moduli space. Once we have fixed the topology and the labeling of zeros and edges (Figures 1 and 2 and Equ.(1.5)) in the z coordinate, we must describe separately the cases where ℓ_7, ℓ_8 or ℓ_9 respectively, are zero. Since we have now only three real degrees of freedom we can fix ξ_1 and only one real component of ξ_2, for example

$$(\zeta|\xi_2) \equiv \mathrm{Re}\,\zeta\,\mathrm{Re}\,\xi_2 + \mathrm{Im}\,\zeta\,\mathrm{Im}\,\xi_2\,, \tag{3.1}$$

where ζ is a given complex number of unit norm. Once these quantities are fixed, the quadratic differentials with one double zero, satisfying the residue conditions have three real degrees of freedom, which are for example, $\mathrm{Re}\,u$, $\mathrm{Im}\,u$ and $(i\zeta|\xi_2)$, where u is the position of the double zero.

We will thus write

$$\phi(z) = -\frac{(z-u)^2\left(z^4 + P_3(z)\right)}{z^2(z-1)^2(z-\xi_1)^2(z-\xi_2)^2}\,, \tag{3.2}$$

where the cubic polynomial

$$P_3(z) = c_3\,z^3 + c_2\,z^2 + c_1\,z + c_0 \tag{3.3}$$

will be completely determined by the following residue conditions at the finite poles

$$\begin{aligned}
y_0 &\equiv P_3(0) = \frac{\xi_1^2\,\xi_2^2}{u^2} \\
y_1 &\equiv P_3(1) = \left(\frac{(1-\xi_1)(1-\xi_2)}{1-u}\right)^2 - 1 \\
y_2 &\equiv P_3(\xi_1) = \left(\frac{\xi_1(\xi_1-1)(\xi_1-\xi_2)}{\xi_1-u}\right)^2 - \xi_1^4 \\
y_3 &\equiv P_3(\xi_2) = \left(\frac{\xi_2(\xi_2-1)(\xi_2-\xi_1)}{\xi_2-u}\right)^2 - \xi_2^4\,.
\end{aligned} \tag{3.4}$$

The polynomial $P_3(z)$ that satisfies (3.4), can be written as in (2.9). Now if we define

$$\begin{aligned} v_0 &\equiv \frac{y_0}{-\xi_1\,\xi_2} \\ v_1 &\equiv \frac{y_1}{(1-\xi_1)(1-\xi_2)} \\ v_2 &\equiv \frac{y_2}{\xi_1(\xi_1-1)(\xi_1-\xi_2)} \\ v_3 &\equiv \frac{y_3}{\xi_2(\xi_2-1)(\xi_2-\xi_1)}\,, \end{aligned} \tag{3.5}$$

we have that

$$\begin{aligned} P_3(z) &= (v_0+v_1+v_2+v_3)\,z^3 - ((1+s)v_0+sv_1+(1+\xi_2)v_2+(1+\xi_1)v_3)\;z^2 + \\ &\quad + ((s+t)v_0+tv_1+\xi_2 v_2+\xi_1 v_3)\;z + \left(\frac{t}{u}\right)^2\,, \end{aligned} \tag{3.6}$$

where again, $s=\xi_1+\xi_2$ and $t=\xi_1\,\xi_2$. And the quadratic differential is completely determined once we give ξ_1, ξ_2 and u.

The regular pyramid

As we did for the regular configurations, we want to calculate explicitly the Strebel quadratic differentials with one double zero in the most symmetric case, a pyramid with a square base (with edges of length $\frac{\pi}{2}$) and four triangles with edges of lengths $\frac{\pi}{2}$, $\frac{3\pi}{4}$ and $\frac{3\pi}{4}$. Again, it is easier to solve the quadratic differential in another coordinate w, where the symmetry is obvious, and then map it to the z-plane. We will have three different mappings h_1, h_2 and h_3, whether the vanishing length is ℓ_8, ℓ_9 or ℓ_7 respectively. In the w coordinate we set the double zero $u=0$ and four poles around it, namely at 1, i, -1 and $-i$. The last pole, corresponding to the base of the pyramid, is at $w=\infty$. By symmetry (see top of Figure 3), we can then immediately read off the ansatz for the zeros w_i, $i=1\ldots 4$ of $\phi(w)$, namely

$$w_1=\alpha e^{-\frac{i\pi}{4}} \quad , \quad w_2=\alpha e^{-\frac{3i\pi}{4}} \quad , \quad w_3=\alpha e^{\frac{3i\pi}{4}} \quad , \quad w_4=\alpha e^{\frac{i\pi}{4}}\,, \tag{3.7}$$

where α is a real positive number. We have thus

$$\phi(w) = -\frac{w^2(w^4+\alpha^4)}{(w^4-1)^2}\,. \tag{3.8}$$

The residue condition at the pole $w=1$ gives us

$$\frac{1+\alpha^4}{16}=1 \quad \Rightarrow \quad \alpha=(15)^{\frac{1}{4}}\,. \tag{3.9}$$

We now map it in the z-plane to the configuration (lower left of Figure 3) which has $\ell_8=0$. The map is

$$z=h_1(w)=\frac{w-1}{w+1}\,. \tag{3.10}$$

This maps the double zero to

$$u^{(1)}=h_1(0)=-1\,, \tag{3.11}$$

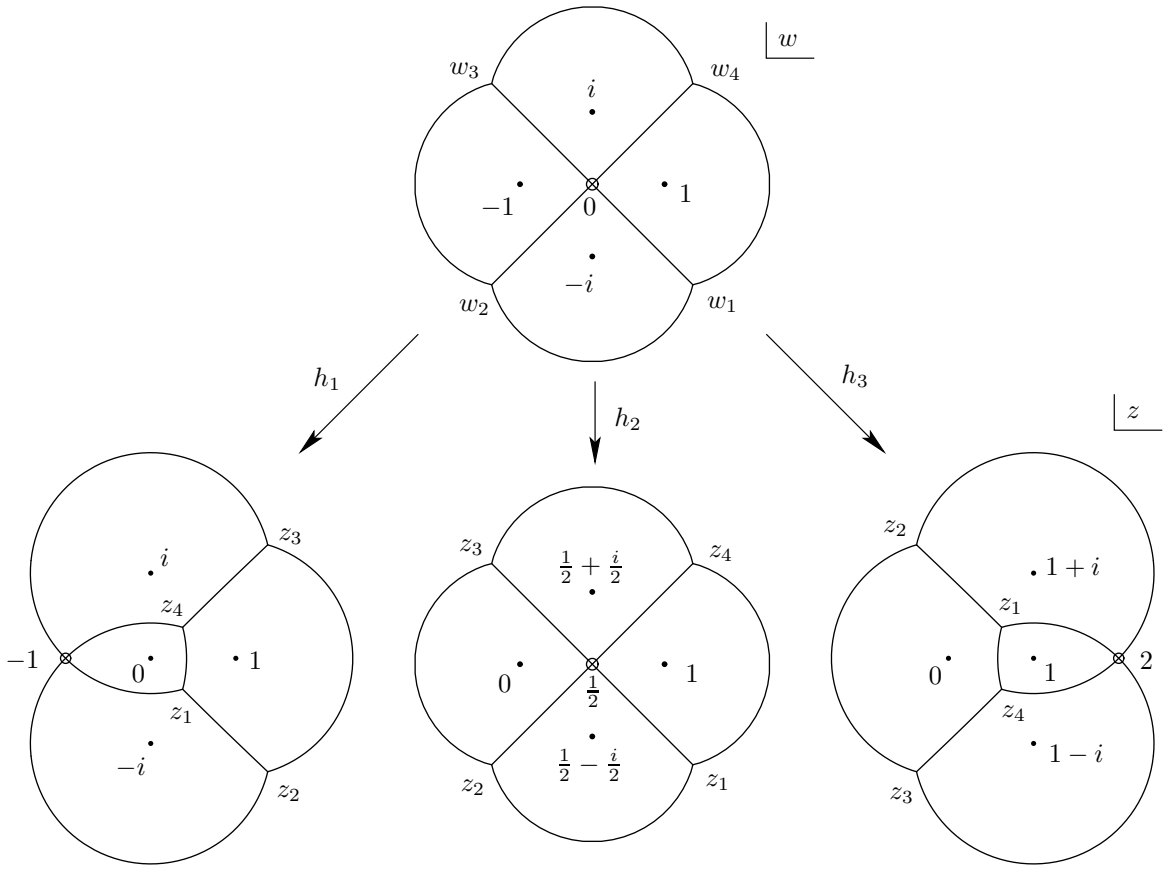

Figure 3: The regular pyramid in the w-plane and its three mappings to the z-plane with respectively $\ell_8 = 0$, $\ell_9 = 0$ and $\ell_7 = 0$. The double zero is marked with a small circle.

and the poles are

$$\xi_1^{(1)} = h_1(i) = i \quad , \quad \xi_2^{(1)} = h_1(-i) = -i\,. \tag{3.12}$$

And the quadratic differential is

$$\phi^{(1)}(z) = -\frac{(z+1)^2\left(z^4 - \frac{7}{2}z^3 + 6z^2 - \frac{7}{2}z + 1\right)}{z^2(z-1)^2(z+i)^2(z-i)^2}\,. \tag{3.13}$$

For the configuration with $\ell_9 = 0$ (lower middle of Figure 3), we have

$$\begin{aligned}
h_2(w) &= \frac{1}{2}(w+1) \\
u^{(2)} &= \frac{1}{2} \\
\xi_1^{(2)} &= \frac{1}{2}(1+i) \quad , \quad \xi_2^{(2)} = \frac{1}{2}(1-i) \\
\phi^{(2)}(z) &= -\frac{\left(z-\frac{1}{2}\right)^2\left(z^4 - 2z^3 + \frac{3}{2}z^2 - \frac{1}{2}z + 1\right)}{z^2(z-1)^2\left(z-\frac{1}{2}(1+i)\right)^2\left(z-\frac{1}{2}(1-i)\right)^2}\,.
\end{aligned} \tag{3.14}$$

And for the configuration with $\ell_7 = 0$ (lower right of Figure 3), we have

$$\begin{aligned} h_3(w) &= \frac{2}{w+1} \\ u^{(3)} &= 2 \\ \xi_1^{(3)} &= 1+i \quad , \quad \xi_2^{(3)} = 1-i \\ \phi^{(3)}(z) &= -\frac{(z-2)^2\left(z^4 - \frac{1}{2}z^3 + \frac{3}{2}z^2 - 2z + 1\right)}{z^2(z-1)^2\left(z-(1+i)\right)^2\left(z-(1-i)\right)^2}\,. \end{aligned} \tag{3.15}$$

It is very useful to have these three exact quadratic differentials to start the Newton method when plotting the boundaries of the second kind.

3.2 Quadratic differentials with two double zeros

As we will see in Section 5, it is important to be able to construct quadratic differentials with two double zeros. In the present section we will see that we can actually solve the Strebel condition in terms of an algebraic curve, i.e. everything can be done algebraically except for a root of a polynomial of order six, which must be found numerically.

From Figure 1 and the lengths conditions (1.5), we see that when the quadratic differential has two double zero, one face must have only two sides (which must therefore have length π). It can then be further deduced that only one length is free, with value ℓ. The other lengths are respectively ℓ, $\pi - \ell$ (two edges) and π. We now look at the quadratic differential in the w-plane where the puncture at infinity is attached to the face with two edges, and the punctures of the other two faces which have these edges as a side are mapped to $w = -1$ and $w = 1$. It is readily seen that in this coordinate, the critical graph must have the symmetry $w \to -w$. This is shown on Figure 4. The two remaining punctures will then be at, say, $w = \alpha$ and $w = -\alpha$. The two

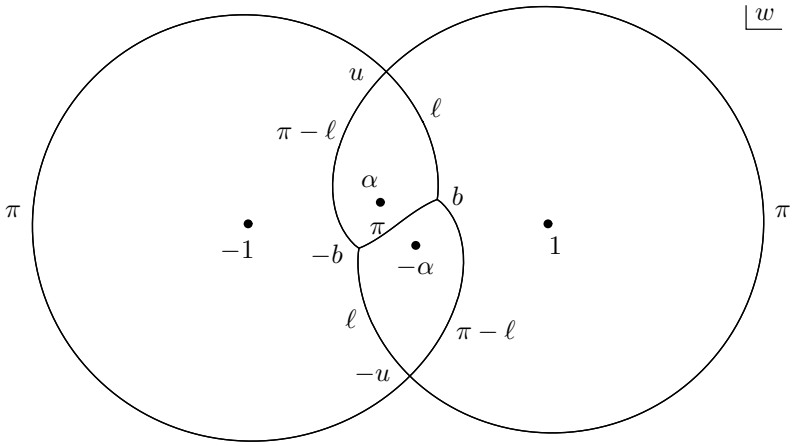

Figure 4: The configuration with two double zeros in the w-plane with the particular value $\ell = 0.8$. The length of each edge is shown.

double zeros are at $w = u$ and $w = -u$, and the two simple zeros are at $w = b$ and $w = -b$. Given the length ℓ, we want to determine the three complex numbers α, u and b.

The quadratic differential $\varphi = \phi(w)(dw)^2$ for this configuration is

$$\phi(w) = -\frac{(w-u)^2\,(w+u)^2\,(w-b)\,(w+b)}{(w-1)^2\,(w+1)^2\,(w-\alpha)^2\,(w+\alpha)^2} = -\frac{(w^2-u^2)^2\,(w^2-b^2)}{(w^2-1)^2\,(w^2-\alpha^2)^2}\,. \tag{3.16}$$

The residue condition at infinity is automatically satisfied by the expression (3.16), and by symmetry the residue condition at $w=-1$ is the same as for $w=1$, and the condition at $w=-\alpha$ is the same as the one at $w=\alpha$. We thus have only two independent residue conditions, at $w=1$ and $w=\alpha$ respectively, which read

$$\frac{(1-u^2)^2\,(1-b^2)}{4\,(1-\alpha^2)^2} = 1 \tag{3.17}$$

$$\frac{(\alpha^2-u^2)^2\,(\alpha^2-b^2)}{4\,\alpha^2\,(1-\alpha^2)^2} = 1\,. \tag{3.18}$$

We are now going to solve the Strebel condition. For this, we need to write that the complex lengths between any two zeros are real. By symmetry, this is automatically satisfied if one length, say the length between b and u, is real. We therefore impose

$$\ell \equiv \ell(b,u) \in \mathbb{R}\,, \tag{3.19}$$

where

$$\ell(b,u) = \int_b^u \frac{(w^2-u^2)\,\sqrt{b^2-w^2}}{(1-w^2)\,(w^2-\alpha^2)}\,dw\,. \tag{3.20}$$

And in total we have two complex equations and one real equation to determine six real parameters, we thus have one free real parameter for the configurations with two double zeros. We take this parameter to be $\ell \in [0,\pi/2]$. The other values $\ell \in [\pi/2,\pi]$ are trivially related to the first case by complex conjugation.

The integral in (3.20) can be calculated by doing the substitution $y = \sqrt{1-\frac{b^2}{w^2}}$, whereby

$$\begin{aligned}
&\int \frac{(w^2-u^2)\,\sqrt{b^2-w^2}}{(1-w^2)\,(w^2-\alpha^2)}\,dw = -i\left(\frac{bu}{\alpha}\right)^2 \int \frac{y^2\left(y^2-\left(1-\frac{b^2}{u^2}\right)\right)}{(y^2-1)\,(y^2-(1-b^2))\left(y^2-\left(1-\frac{b^2}{\alpha^2}\right)\right)}\,dy \\
&= i\int\left(\frac{1}{y^2-1} - 2\frac{\sqrt{1-b^2}}{y^2-(1-b^2)} + 2\frac{\sqrt{1-\frac{b^2}{\alpha^2}}}{y^2-\left(1-\frac{b^2}{\alpha^2}\right)}\right)\,dy \\
&= \frac{i}{2}\ln\left(\frac{\left(\sqrt{1-\frac{b^2}{w^2}}-1\right)\left(\sqrt{1-\frac{b^2}{w^2}}+\sqrt{1-b^2}\right)^2\left(\sqrt{1-\frac{b^2}{w^2}}-\sqrt{1-\frac{b^2}{\alpha^2}}\right)^2}{\left(\sqrt{1-\frac{b^2}{w^2}}+1\right)\left(\sqrt{1-\frac{b^2}{w^2}}-\sqrt{1-b^2}\right)^2\left(\sqrt{1-\frac{b^2}{w^2}}+\sqrt{1-\frac{b^2}{\alpha^2}}\right)^2}\right)\,.
\end{aligned} \tag{3.21}$$

To go from the first to the second line we have made use of the residue conditions (3.17) and (3.18). So the length between b and u is

$$\ell = \frac{\pi}{2} + \frac{i}{2}\ln\left(\frac{\left(\sqrt{1-\frac{b^2}{u^2}}-1\right)\left(\sqrt{1-\frac{b^2}{u^2}}+\sqrt{1-b^2}\right)^2\left(\sqrt{1-\frac{b^2}{u^2}}-\sqrt{1-\frac{b^2}{\alpha^2}}\right)^2}{\left(\sqrt{1-\frac{b^2}{u^2}}+1\right)\left(\sqrt{1-\frac{b^2}{u^2}}-\sqrt{1-b^2}\right)^2\left(\sqrt{1-\frac{b^2}{u^2}}+\sqrt{1-\frac{b^2}{\alpha^2}}\right)^2}\right)\,.$$

It is natural to make the definitions

$$s \equiv \sqrt{1-\frac{b^2}{u^2}} \quad , \qquad t \equiv \sqrt{1-b^2} \quad , \qquad v \equiv \sqrt{1-\frac{b^2}{\alpha^2}}\,. \tag{3.22}$$

We thus have

$$\frac{(s-1)(s+t)^2(s-v)^2}{(s+1)(s-t)^2(s+v)^2} = e^{i(\pi-2\ell)}\,. \tag{3.23}$$

We note that the equations (3.17) and (3.18) give us a simple relation between t and v

$$t - v = -\frac{1}{2}tv\,. \tag{3.24}$$

It will be convenient to define

$$T \equiv tv\,. \tag{3.25}$$

The following identities follow directly from (3.24)

$$t = \sqrt{\frac{T^2}{16}+T} - \frac{T}{4} \quad , \qquad v = \sqrt{\frac{T^2}{16}+T} + \frac{T}{4}\,. \tag{3.26}$$

We also have from (3.17), (3.22) and (3.26)

$$s^2 = -\frac{3T(T-4)}{4(1+T)}\,, \tag{3.27}$$

and

$$u = \frac{ib}{\sqrt{s^2-1}} \quad , \qquad \alpha = \frac{ib}{\sqrt{v^2-1}}\,. \tag{3.28}$$

Let us now rewrite (3.23) as a polynomial equation in s, whose coefficients are expressed in terms of T and ℓ with the help of (3.26)

$$-i\cot(\ell)\,s^5 - (1+T)s^4 - i\cot(\ell)\,\left(\frac{T^2}{4}-T\right)s^3 + \left(\frac{3}{4}T^2+2T\right) - T^2 = 0\,. \tag{3.29}$$

Using (3.27) this becomes

$$s = -\frac{i}{3}\tan(\ell)\,\frac{18(T+1)\left(T-\frac{16}{9}\right)}{(T-4)^2} \tag{3.30}$$

Squaring and using again (3.27), we finally get a polynomial equation for T.

$$P_\ell(T) \equiv -\cot^2(\ell)\,T(T-4)^5 + 48(T+1)^3\left(T-\frac{16}{9}\right)^2 = 0\,. \tag{3.31}$$

We immediately see the solutions of this equation for the particular values $\ell = \pi/2$ and $\ell \to 0$. Namely $T = 16/9$ and $T = 4$ respectively. For generic ℓ, this equation must be solved numerically, following the branch $T(\ell = \pi/2) = 16/9$.

We would like to characterize precisely the branch of the solution of (3.31) that we must choose. We start by showing that the branches cross only at the points $T = \frac{16}{9}$ and $T = 4$. Branches cross at multiple zeros, when $P_\ell(T)$ and $P'_\ell(T)$ vanish simultaneously. We have

$$P'_\ell(T) = (3T-2)\left(-2\,\cot^2(\ell)(T-4)^4 + \frac{5}{3}\,48(T+1)^2\left(T-\frac{16}{9}\right)\right). \tag{3.32}$$

We define

$$A \equiv -\cot^2(\ell)(T-4)^4 \qquad , \qquad B \equiv 48(T+1)^2\left(T-\frac{16}{9}\right), \tag{3.33}$$

so that we have the system

$$0 \;=\; P_\ell(T) = T(T-4)\,A + (T+1)\left(T-\frac{16}{9}\right)B \tag{3.34}$$

$$0 \;=\; P'_\ell(T) = (3T-2)\left(2\,A + \frac{5}{3}\,B\right). \tag{3.35}$$

Let us look at the second equation. If $T = \frac{2}{3}$, (3.31) tells us that $\cot^2(\ell) = -1$. If $T \neq \frac{2}{3}$, we must have $B = -\frac{6}{5}A$, and the first equation tells us that either $T = \frac{2}{3}$ or $T = -16$. In both of these cases we see from (3.31), that $\cot^2(\ell) = -1$. We have thus shown that the branches do not cross when $\ell \in (0, \frac{\pi}{2})$. From this fact we can completely derive the topology of the branch diagram (by which we mean the locus in the T-plane formed by all roots of $P_\ell(T)$ for all $\ell \in [0, \frac{\pi}{2}]$). Since the polynomial $P_\ell(T)$ is real, the branch diagram must be symmetric under complex conjugation. Five branches must start (at $\ell = 0$) from $T = 4$ and one must start from $T = 0$, whereas three branches end (when $\ell = \frac{\pi}{2}$) at $T = -1$ and two must end at $T = \frac{16}{9}$. Also when $\ell \to \frac{\pi}{2}$, $\cot^2(\ell)$ tends to zero and we have a solution

$$T \approx \frac{48}{\cot^2(\ell)} \to +\infty\,,$$

and therefore one branch must end at $+\infty$. It is then clear that the only topology compatible with all these observations is the one shown on Figure 5. The branch corresponding to the conventions of Figure 4 is the one drawn with a bold line. It can be characterized by the fact that it belongs to the rectangle $\frac{16}{9} \le \mathrm{Re}\,T \le 4$ and $-0.6 \le \mathrm{Im}\,T \le 0$. We will thus define the function $T(\ell)$ by

$$\boxed{T(\ell) \text{ is the unique solution of } \begin{cases} -\cot^2(\ell)\,T(T-4)^5 + 48(T+1)^3\left(T-\frac{16}{9}\right)^2 = 0 \\ \frac{16}{9} \le \mathrm{Re}\,T \le 4 \\ -0.6 \le \mathrm{Im}\,T \le 0 \end{cases}} \tag{3.36}$$

From (3.22), (3.26) and (3.28), we can write the expressions of $b(\ell)$, $u(\ell)$ and $\alpha(\ell)$ in terms of $T(\ell)$. The only one we will need is $\alpha(\ell)$

$$\alpha(\ell) = i\,\frac{1 - \frac{T(\ell)^2}{8} - T(\ell) + \frac{T(\ell)}{2}\sqrt{\frac{T(\ell)^2}{16} + T(\ell)}}{\sqrt{2T(\ell) - 1 - \frac{3}{4}T(\ell)^2}}\,. \tag{3.37}$$

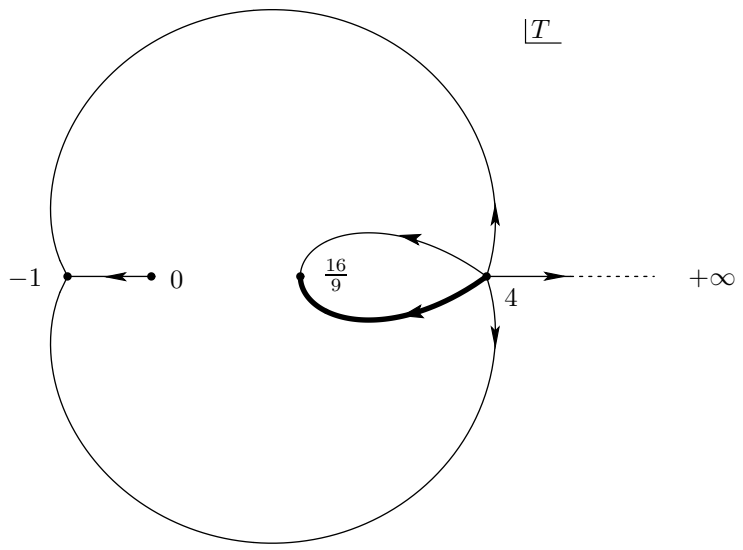

Figure 5: The branch structure of Equ.(3.31). The branch chosen is the bold one.

This expression will be useful later do describe the boundary of the projection of the reduced moduli space on the ξ_1-plane. We already note the special values

$$\alpha(0) = 2 - \sqrt{5} \quad , \qquad \alpha(\pi/2) = \frac{27}{32\sqrt{6} + 19\sqrt{15}}\, i\,. \tag{3.38}$$

4 Solving a quadratic differential numerically

We now want to describe the numerical algorithm to solve a quadratic differential. We will focus on the regular quadratic differentials, but the techniques can be applied, with only trivial modifications, to quadratic differentials with one double zero. We will then recall how to compute the mapping radii, and we'll shortly discuss how we compute derivatives with respect to ξ_i and $\bar{\xi}_i$.

The central problem is to find, for given poles ξ_1 and ξ_2, the quadratic differential (i.e. its parameters a_1 and a_2) that satisfies the Strebel condition. In other words its critical graph must close, with its zeros being linked with horizontal trajectories. We remind that horizontal trajectories are defined by the condition $\phi(z)(dz)^2 > 0$, so the Strebel condition is equivalent to the condition that all the complex lengths between zeros, z_i and z_f, are real.

$$\mathrm{Im}\,\ell(z_i, z_f) = \mathrm{Im}\int_{z_i}^{z_f} \sqrt{\phi(z)}\, dz = 0 \quad , \quad i, f = 1, \ldots, 6\,. \tag{4.1}$$

We have nine lengths (see Figure 2) constrained by the five residue conditions; this leaves us four independent lengths, which we can choose as ℓ_6, ℓ_4, ℓ_9 and ℓ_2 (as labeled on Figure 2). We thus have to solve a system of four real equations of four real unknowns

$$\mathbf{f}(\mathbf{x}) = 0\,, \tag{4.2}$$

with $\mathbf{f} = (\operatorname{Im}\ell_6, \operatorname{Im}\ell_4, \operatorname{Im}\ell_9, \operatorname{Im}\ell_2)^T$ and $\mathbf{x} = (\operatorname{Re}a_1, \operatorname{Im}a_1, \operatorname{Re}a_2, \operatorname{Im}a_2)^T$. We use Newton's method

$$\mathbf{x}_{i+1} = \mathbf{x}_i - \left(\frac{\partial \mathbf{f}}{\partial \mathbf{x}}\right)^{-1} \cdot \mathbf{f}(\mathbf{x}_i)\,, \tag{4.3}$$

which converges when the initial guess $\mathbf{x}_0$ is not too far from the solution. The Jacobian $\partial\mathbf{f}/\partial\mathbf{x}$ can be expressed in terms of derivatives with respect to a_i

$$\frac{\partial \mathbf{f}}{\partial \mathbf{x}} = \begin{pmatrix} \operatorname{Im}\partial_{a_1}\ell_6 & \operatorname{Re}\partial_{a_1}\ell_6 & \operatorname{Im}\partial_{a_2}\ell_6 & \operatorname{Re}\partial_{a_2}\ell_6 \\ \operatorname{Im}\partial_{a_1}\ell_4 & \operatorname{Re}\partial_{a_1}\ell_4 & \operatorname{Im}\partial_{a_2}\ell_4 & \operatorname{Re}\partial_{a_2}\ell_4 \\ \operatorname{Im}\partial_{a_1}\ell_9 & \operatorname{Re}\partial_{a_1}\ell_9 & \operatorname{Im}\partial_{a_2}\ell_9 & \operatorname{Re}\partial_{a_2}\ell_9 \\ \operatorname{Im}\partial_{a_1}\ell_2 & \operatorname{Re}\partial_{a_1}\ell_2 & \operatorname{Im}\partial_{a_2}\ell_2 & \operatorname{Re}\partial_{a_2}\ell_2 \end{pmatrix} \tag{4.4}$$

We continue this section by explaining how to accurately compute numerically the complex lengths and their derivatives with respect to a_i. And we will continue by describing the computation of the mapping radii, and of the derivatives of a_i with respect to ξ_j and $\bar{\xi}_j$.

4.1 The complex lengths

The quintic numerical computation turns out to be very much harder than the quartic. In the quartic computation [7], there were two weaknesses which had negligible consequences. First it was hard to tell if the path of integration (which was chosen to be a straight line) was going on the right side of the poles, hence a possible ambiguity of $2\pi\, n$ in the length. Combined with the sign ambiguity of the square root, there was a potential problem when the length was nearly π. Although we could go around this ambiguity in the quartic case, for the quintic calculation it would be catastrophic. Second, we used the coded "continuous square root", which remembers its last evaluation and tries to detect if the branch cut has been crossed between the last two evaluations. Again this is not good enough in the quintic case; we would inevitably encounter situations when the continuous square root fails to detect a branch cut, again with catastrophic consequences.

To solve the first problem, we make a conjecture based on observation that the integration path between two zeros z_i and z_f along the critical trajectory C that connects them, can be continuously deformed to the path shown on Figure 6, z_i to p_j to z_f without crossing any pole (other than p_j). Here p_j is a pole such that the zeros z_i and z_f are on the boundary of its ring domain.

$$\ell(z_i, z_f) = \int_C \sqrt{\phi(z)}\, dz = \int_{z_i}^{z_1} \sqrt{\phi(z)}\, dz + \int_S \sqrt{\phi(z)}\, dz + \int_{z_2}^{z_f} \sqrt{\phi(z)}\, dz\,.$$

For numerical reasons that will become clear in a while, we split the integrals along the straight lines in two, by setting $m_1 = \frac{1}{2}(z_i + p_j)$ and $m_2 = \frac{1}{2}(z_f + p_j)$, and writing

$$\ell(z_i, z_f) = \int_{z_i}^{m_1} \sqrt{\phi(z)}\, dz + \int_{m_1}^{z_1} \sqrt{\phi(z)}\, dz + \int_S \sqrt{\phi(z)}\, dz + \int_{z_2}^{m_2} \sqrt{\phi(z)}\, dz + \int_{m_2}^{z_f} \sqrt{\phi(z)}\, dz\,. \tag{4.5}$$

Now we subtract the poles at $z = p_j$ in the integrals from m_k to z_k, and put them back together

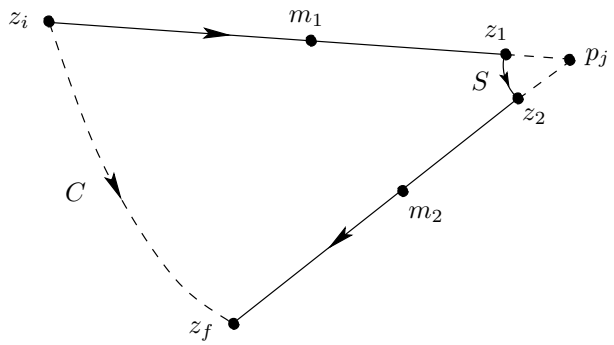

Figure 6: The critical trajectory C can always be deformed continuously to the contour integration shown with solid lines.

with the integral over S, and we take the limit $z_1, z_2 \to p_j$.

$$\begin{aligned}\ell(z_i, z_f) &= \int_{z_i}^{m_1} \sqrt{\phi(z)}\, dz - \int_{z_f}^{m_2} \sqrt{\phi(z)}\, dz \\ &+ \int_{m_1}^{p_j} \left(\sqrt{\phi(z)} - \frac{r}{z-p_j} \right) dz - \int_{m_2}^{p_j} \left(\sqrt{\phi(z)} - \frac{r}{z-p_j} \right) dz \\ &+ \lim_{\substack{z_1, z_2 \to p_j \\ |z_1 - p_j| = |z_2 - p_j|}} \left(\int_S \sqrt{\phi(z)}\, dz + r \int_{m_1}^{z_1} \frac{1}{z-p_j}\, dz - r \int_{m_2}^{z_2} \frac{1}{z-p_j}\, dz \right), \end{aligned} \tag{4.6}$$

where $r = \pm i$ is the residue of $\sqrt{\phi(z)}$ at $z = p_j$. It is now time to define $\sqrt{\phi(z)}$. We want it to be continuous on the integration path, in other words, we don't want to cross any branch cut. The idea is to calculate the intersection of the integration path with the branch cut of the conventional square root, and then change the sign according to the number $n(z)$ of branch points that were crossed. Since $\phi(z)$ is given by an expression of the form

$$\phi(z) = \frac{-P(z)}{D(z)^2}\,, \tag{4.7}$$

we write

$$\sqrt{\phi(z)} \equiv \frac{\sqrt{-\eta^2 P(z)}}{\eta D(z)} (-1)^{n(z)}\,, \tag{4.8}$$

where the square root on the right hand side is the conventional square root with branch cut the negative real axis. We ignore η for now and focus on $n(z)$. When z_0 is on the integration path, say $[z_i, p_j]$, we define $n(z_0)$ to be the number of times that the conventional square root $\sqrt{-\eta^2 P(y)}$ crosses its branch cut when $y \in [z_0, p_j]$, In particular $n(p_j) = 0$. We start by parameterizing the path with $t \in [-1, 1]$

$$z(t) = \frac{p_j - z_i}{2}\, t + \frac{p_j + z_i}{2} \equiv az + b\,, \tag{4.9}$$

$n(z_0)$ is then given by the number of solutions t_i of the equation

$$\mathrm{Im}\left(-\eta^2 P(z(t_i))\right) = 0\,, \tag{4.10}$$

satisfying the conditions

$$\mathrm{Re}\left(-\eta^2 P(z(t_i))\right) < 0 \qquad \text{and} \qquad t_0 < t_i < 1\,, \tag{4.11}$$

where $z(t_0) = z_0$. It is then clear that (4.8) will be continuous. Let us now look at the complex number η in (4.8). We want to choose it in such a way that the residue of $\sqrt{\phi(z)}$ at $z = p_j$, which is $\pm i$, takes the negative sign. Remembering that the "residues" of $\phi(z)$ at the poles are -1, we see that $P(p_j) = \prod_{i\neq j}(p_j - p_i)^2 = (D'(p_j))^2$. We thus require that η satisfies

$$\frac{\sqrt{-\left(\eta D'(p_j)\right)^2}}{\eta D'(p_j)} = -i\,, \tag{4.12}$$

which is the case if

$$\mathrm{Im}\left(\eta D'(p_j)\right) > 0 \qquad \text{or} \qquad \left(\mathrm{Im}\left(\eta D'(p_j)\right) = 0 \quad \text{and} \quad \mathrm{Re}\left(\eta D'(p_j)\right) < 0\right)\,. \tag{4.13}$$

We will therefore take (demanding also that η has unit norm)

$$\eta = i\,\frac{|D'(p_j)|}{D'(p_j)}\,e^{i\theta}\,, \tag{4.14}$$

where $\theta \in (-\frac{\pi}{2}, \frac{\pi}{2})$ can be chosen arbitrarily, as long as as it is not zero. Indeed if $\theta = 0$, we would have $-\eta^2 P(p_j) > 0$, and (4.10) would have the solution $t = 1$. This must be avoided because, due to numerical uncertainties, we would find a solution $t = 1 \pm \epsilon$ and it would be hard to decide whether to count it in $n(z)$ or not. If $\theta \neq 0$, we avoid this problem.

We can now continue the computation (4.6) by setting $r = -i$. In the limit considered, the integral over the arc of circle S is just a bit of the residue, namely

$$\int_S \sqrt{\phi(z)}dz = \alpha i(-i) = \alpha\,, \tag{4.15}$$

where α is the angle at the tip p_j of the triangle $z_i p_j z_f$. We thus have

$$\int_S \sqrt{\phi(z)}dz = \arg^*\frac{z_f - p_j}{z_i - p_j}\,, \tag{4.16}$$

where $\arg^*$ is the argument function with range $[0, 2\pi)$, in other words, its branch cut is on the positive real axis. This is necessary because α might be greater than π, when p_j is on the right of the straight line from z_i to z_f but still on the left of the path C. The last two integrals in (4.6) give

$$\begin{aligned}
&\lim_{\substack{z_1,z_2\to p_j \\ |z_1-p_j|=|z_2-p_j|}} \left(-i\int_{m_1}^{z_1}\frac{1}{z-p_j}\,dz + i\int_{m_2}^{z_2}\frac{1}{z-p_j}\,dz\right) \\
&= -i \lim_{\substack{z_1,z_2\to p_j \\ |z_1-p_j|=|z_2-p_j|}} \log\left(\frac{z_1-p_j}{z_2-p_j}\frac{z_f-p_j}{z_i-p_j}\right) = -i\log\left|\frac{z_f-p_j}{z_i-p_j}\right|\,,
\end{aligned} \tag{4.17}$$

where in the last equality, we used the fact that z_1 is on the segment from z_i to p_j and z_2 is on the segment from z_f to p_j, and the argument of the log is therefore a positive real number. Combining (4.16) and (4.17), we see that the last line of (4.6) is

$$-i\log^*\frac{z_f - p_j}{z_i - p_j}\,,$$

where $\log^* z \equiv \log|z| + i \arg^* z$. In total we have therefore

$$\begin{aligned}\ell(z_i, z_f) &= \int_{z_i}^{m_1} \sqrt{\phi(z)}\, dz + \int_{m_1}^{p_j} \left(\sqrt{\phi(z)} + \frac{i}{z-p_j}\right) dz \\ &\quad - \left(\int_{z_f}^{m_2} \sqrt{\phi(z)}\, dz + \int_{m_2}^{p_j} \left(\sqrt{\phi(z)} + \frac{i}{z-p_j}\right) dz\right) - i\, \log^* \frac{z_f - p_j}{z_i - p_j}\,. \end{aligned} \tag{4.18}$$

We shall now explain why we have split in two the integrals along the straight lines. For this we need to make a parenthesis into the Gaussian quadrature formulas (see for example [17]) which we use to compute numerically the integrals in (4.18). Those are very useful when integrating, over the finite interval $[-1, 1]$, a function $g(t)$ that behaves like $(1-t)^\alpha$ near $t = 1$, and like $(1+t)^\beta$ near $t = -1$, where $\alpha, \beta > -1$. If α or β are not integer the function $g(t)$ will have singular derivatives, and a quadrature formula like the trapezoidal method or the Gauss method with no weight (which is adapted when $\alpha = \beta = 0$) will give inaccurate results. In that case, we need to use the Gauss-Jacobi quadrature formula

$$\int_{-1}^{1} (1-t)^\alpha (1+t)^\beta f(t) dt = \sum_{j=1}^{N} H_j f(a_j) + E\,, \tag{4.19}$$

where

$$g(t) = (1-t)^\alpha (1+t)^\beta f(t)\,, \tag{4.20}$$

and $f(t)$ is infinitely differentiable with all its derivatives bounded on $[-1, 1]$. The abscissas a_j are the roots of the Jacobi polynomial $J_N(t; \alpha, \beta)$, the weights H_j are given by

$$H_j = -\frac{2N+\alpha+\beta+2}{N+\alpha+\beta+1} \frac{\Gamma(N+\alpha+1)\Gamma(N+\beta+1)}{\Gamma(N+\alpha+\beta+1)(N+1)!} \frac{2^{\alpha+\beta}}{J'_N(a_j;\alpha,\beta) J_{N+1}(a_j;\alpha,\beta)}\,, \tag{4.21}$$

and the error E is

$$E = \frac{\Gamma(N+\alpha+1)\Gamma(N+\beta+1)\Gamma(N+\alpha+\beta+1)}{(2N+\alpha+\beta+1)\left(\Gamma(2N+\alpha+\beta+1)\right)^2} \frac{N! 2^{2N+\alpha+\beta+1}}{(2N)!} f^{(2N)}(\zeta) \quad , \quad \zeta \in (-1, 1). \tag{4.22}$$

Now suppose that we didn't split the integrals in (4.5) and tried to integrate

$$\int_{-1}^{1} \left(\sqrt{\phi(z(t))} + \frac{i}{z(t) - p_j}\right) dt\,.$$

At $t = -1$, the first term behave like $(t+1)^{1/2}$, but because of the second term, we cannot write the integrand in the form (4.20). This is why we had to split the integrals in (4.5). In this way, the first and third integrals in (4.18) are of the form (4.20) with $\alpha = 0$ and $\beta = \frac{1}{2}$, while the second and fourth integrals have $\alpha = \beta = 0$.

Note that there is an alternative to the splitting, which was used in [7]. It is to subtract to $\sqrt{\phi(z)}$ the expression

$$\frac{-i}{\sqrt{2}} \frac{\sqrt{t+1}}{(z(t) - p_j)}$$

instead of $-i/(z(t)-p_j)$. In that way we can factor out the square root along the whole path. But we find the splitting method easier, because the expression

$$\sqrt{\phi(z)}+\frac{i}{z-p_j}$$

is simpler when one simplifies it by explicitly canceling the poles. What we mean is that this expression is prone to numerical errors, because when z is close to p_j we are subtracting two large and almost equal numbers, a cancellation error. So we need to manipulate this expression. Namely

$$\begin{aligned}\sqrt{\phi(z)}+\frac{i}{z-p_j} &= \frac{\sqrt{-\eta^2 P(z)}}{\eta D(z)}+\frac{i}{z-p_j}=\frac{\sqrt{-\eta^2 P(z)}+i\eta D_j(z)}{\eta D(z)} \\ &= \eta\frac{D_j(z)^2-P(z)}{z-p_j}\,\left(D_j(z)\left(\sqrt{-\eta^2 P(z)}-i\eta D_j(z)\right)\right)^{-1}, \end{aligned} \tag{4.23}$$

where we have defined

$$D_j(z)\equiv\frac{D(z)}{z-p_j}=\prod_{i\neq j}(z-p_i)\,. \tag{4.24}$$

We can cancel the apparent pole in the factor

$$Q(z)\equiv\frac{D_j(z)^2-P(z)}{z-p_j} \tag{4.25}$$

because the residue condition of the quadratic differential at its poles implies that $P(p_j)=D_j(p_j)^2$, so the numerator of (4.25) is a polynomial with a factor $z-p_j$. Thus $Q(z)$ is a polynomial, and the right hand side of (4.23) is well defined, analytically as well as numerically.

In order to use the Newton method, we still need to calculate the derivatives $\partial_{a_j}\ell(z_i,z_f)$. Since $\phi(z)$ vanishes at the endpoints of the integration path, we can simply differentiate inside the integral

$$\frac{\partial}{\partial a_j}\ell(z_i,z_f)=\frac{\partial}{\partial a_j}\int_C\sqrt{\phi(z)}\,dz=\frac{1}{2}\int_C\frac{1}{\sqrt{\phi(z)}}\frac{\partial\phi(z)}{\partial a_j}\,dz\,. \tag{4.26}$$

With the expressions (2.14) for the derivatives and the definition (4.8) of the square root, and deforming the integration contour as before we find

$$\begin{aligned}\frac{\partial}{\partial a_1}\ell(z_i,z_f) &= -\frac{\eta}{2}\left(\int_{z_i}^{p_j}\frac{(-1)^{n(z)}}{\sqrt{-\eta^2P(z)}}\,dz-\int_{z_f}^{p_j}\frac{(-1)^{n(z)}}{\sqrt{-\eta^2P(z)}}\,dz\right) \\ \frac{\partial}{\partial a_2}\ell(z_i,z_f) &= -\frac{\eta}{2}\left(\int_{z_i}^{p_j}\frac{z\,(-1)^{n(z)}}{\sqrt{-\eta^2P(z)}}\,dz-\int_{z_f}^{p_j}\frac{z\,(-1)^{n(z)}}{\sqrt{-\eta^2P(z)}}\,dz\right). \end{aligned} \tag{4.27}$$

These integrals can be evaluated accurately with a Gauss-Jacobi formula with $\alpha=0$ and $\beta=-\frac{1}{2}$.

4.2 The mapping radii

We recall that the mapping radii ρ_j appear as a multiplicative factor in front of the local coordinate w_j in the power expansion of the maps h_j from the local coordinates to the uniformizer z (or $t = 1/z$ for the puncture at infinity) (see Equ.(7.26)). While all other terms in the expansion can be determined by expanding the quadratic differential, the mapping radii can't. Instead, they must be computed by integrating $\sqrt{\phi(z)}$ from a point on the boundary of the ring domain of the pole, to the pole p_j, and subtracting the singular logarithm (see [9, 7])

$$\log \rho_j = \lim_{\epsilon \to 0} \left(\mathrm{Im} \int_{z_i}^{p_j + \epsilon\alpha} \sqrt{\phi(z)} dz + \log \epsilon \right) \quad , \quad \alpha = \frac{z_i - p_j}{|z_i - p_j|} \,, \tag{4.28}$$

and we take z_i to be one of the zeros on the boundary of the ring domain. The square root is again defined as in (4.8) with η as in (4.14), so the residue of $\sqrt{\phi(z)}$ at $z = p_j$ is $-i$. This integral is very similar to that for the complex lengths, so we know how to evaluate it numerically. First we break the integration in two and regularize the integrand near the pole

$$\log \rho_j = \lim_{\epsilon \to 0} \left(\mathrm{Im} \int_{z_i}^{z_1} \sqrt{\phi(z)} dz + \mathrm{Im} \int_{z1}^{p_j + \epsilon\alpha} \left(\sqrt{\phi(z)} + \frac{i}{z - p_j} \right) dz + \log \epsilon - \mathrm{Re} \int_{z_1}^{p_j + \epsilon\alpha} \frac{1}{z - p_j} dz \right)$$

where for definiteness we take $z_1 = \frac{1}{2}(z_i + p_j)$. Now we can easily get rid of the limit

$$\begin{aligned} \log \rho_j &= \lim_{\epsilon \to 0} \left(\mathrm{Im} \int_{z_i}^{z_1} \sqrt{\phi(z)} dz + \mathrm{Im} \int_{z_1}^{p_j + \epsilon\alpha} \left(\sqrt{\phi(z)} + \frac{i}{z - p_j} \right) dz - \log \left| \frac{\epsilon\alpha}{z_1 - p_j} \right| + \log \epsilon \right) \\ &= \mathrm{Im} \int_{z_i}^{z_1} \sqrt{\phi(z)} dz + \mathrm{Im} \int_{z_1}^{p_j} \left(\sqrt{\phi(z)} + \frac{i}{z - p_j} \right) dz + \log \left| \frac{z_i - p_j}{2} \right| . \end{aligned} \tag{4.29}$$

The integrand of the second term is manipulated as in (4.23) - (4.25), and both integrals can be evaluated accurately with Gauss-Jacobi quadrature formulas as in the last subsection.

The pole at infinity must be treated separately; we must work in the coordinate $t = 1/z$. The radius is then

$$\log \rho_5 = \lim_{\epsilon \to 0} \left(\mathrm{Im} \int_{1/z_i}^{\epsilon\alpha} \sqrt{\phi(t)} dt + \log \epsilon \right) , \tag{4.30}$$

where z_i is a zero on the boundary of the ring domain at infinity. One could of course rewrite the integral in the z coordinate

$$\int_{1/z_i}^{\epsilon\alpha} \sqrt{\phi(t)} dt = \int_{z_i}^{\frac{1}{\epsilon\alpha}} \sqrt{\phi(z)} dz \,,$$

but we prefer to integrate numerically over a finite interval, so we will stay in the t coordinate. We have thus

$$\begin{aligned} \log \rho_5 &= \lim_{\epsilon \to 0} \left(\mathrm{Im} \int_{\frac{1}{z_i}}^{\frac{1}{2z_i}} \sqrt{\phi(t)} dt + \mathrm{Im} \int_{\frac{1}{2zi}}^{\epsilon\alpha} \left(\sqrt{\phi(t)} + \frac{i}{t} \right) dt + \log \epsilon - \mathrm{Re} \int_{\frac{1}{2z_i}}^{\epsilon\alpha} \frac{1}{t} dt \right) \\ &= \mathrm{Im} \int_{\frac{1}{z_i}}^{\frac{1}{2z_i}} \sqrt{\phi(t)} dt + \mathrm{Im} \int_{\frac{1}{z_i}}^{0} \left(\sqrt{\phi(t)} + \frac{i}{t} \right) dt + \log \left| \frac{1}{2z_i} \right| . \end{aligned} \tag{4.31}$$

The integrand of the second term can be manipulated again, as in (4.23) - (4.25), in order to get rid of the apparent singularity at $t = 0$. It is understood that before doing so one has to express $\phi(t)$ in the coordinate t.

$$\phi(t) = \phi(z = t^{-1}) \, \frac{1}{t^4} \, . \tag{4.32}$$

4.3 The derivatives

In order to compute amplitudes involving not only tachyons, we need the derivatives $\frac{\partial a_i}{\partial \xi_j}$ and $\frac{\partial a_i}{\partial \bar{\xi}_j}$. We don't have expressions for these quantities that we could directly evaluate, so we need to estimate these derivatives. We are using a Richardson's formula of order four, which for a function f differentiable at least five times, reads

$$f'(x) = \frac{1}{6h} \left(f(x-h) - 8f(x-h/2) + 8f(x+h/2) - f(x+h) \right) + \mathcal{O}(h^4) \, . \tag{4.33}$$

As we are working with numbers in double precision (which is usually around 16 significant digits) we see from this formula that the most efficient h is approximately $h = 10^{-3}$, which should give a result accurate to about twelve significant digits; taking a smaller h would reduce the precision because of cancellation errors. If we write $\xi_i = x_i + i \, y_i$, we have $\partial_{\xi_i} = \frac{1}{2}(\partial_{x_i} - i \, \partial_{y_i})$ and $\partial_{\bar{\xi}_i} = \frac{1}{2}(\partial_{x_i} + i \, \partial_{y_i})$, for each a_i we thus need to evaluate the four derivatives $\frac{\partial a_i}{\partial x_j}$ and $\frac{\partial a_i}{\partial y_j}$, $j = 1, 2$. Each derivative calculated with (4.33) requires four evaluation of the function, so in total we need to solve the Strebel differential at sixteen points in order to evaluate accurately its derivatives at a given point. Note that for the quartic vertex [7], the derivatives are calculated ([11, 12, 15]) by differentiating the fit $a^{\text{fit}}(\xi, \bar{\xi})$, but for the quintic we haven't been able to write a reasonably short fit.

5 The reduced moduli space

In this section we describe the boundary of the reduced moduli space $\mathcal{V}_{0,5}$ (which we sometimes call simply moduli space, without ambiguity since we always consider the reduced moduli space), and the methods to evaluate it numerically. To represent this four-dimensional moduli space, we first study its projection on the ξ_1-plane, this can be done algebraically. Then at every point of the projection, we have to describe the two-dimensional section in the ξ_2-plane; we do this numerically.

We naturally want to reduce the numerical part of the problem to the minimum. For this, we need to figure out what is the smallest part of $\mathcal{V}_{0,5}$ that we need to describe numerically and still be able to integrate over the whole $\mathcal{V}_{0,5}$. We can do two successive partitioning of the moduli space. Firstly, let five string states $|\Psi_i\rangle$, $i = 1, \ldots, 5$, scattering on a five-punctured sphere, given by a particular point m of $\mathcal{V}_{0,5}$. We can draw, on the sphere, the critical graph of the Jenkins-Strebel quadratic differential uniquely determined by m. For almost all m (i.e. all $m \in \mathcal{V}_{0,5}$ except for the ones belonging to a subset of measure zero), the graph will delimit a prism consisting of two opposing triangles and three quadrilaterals (see Figure 1); we can thus partition the moduli space into ten regions, according to which three of the five states belong to the quadrilateral faces of

the prism. We conformally map the sphere onto a sphere, requiring that the three quadrilateral vertices are mapped to the standard points $z = 0$, $z = 1$ and $z = \infty$ (there are six such maps, but which one we choose is irrelevant as will become clear below). Secondly, as in the case of the quartic vertex [14, 7], we can use the six $\mathrm{PSL}(2,\mathbb{C})$ transformations that map the set $\{0, 1, \infty\}$ onto itself, and complex conjugation, to partition further the ten regions of $\mathcal{V}_{0,5}$ into twelve parts. In total, the moduli space is thus composed of 120 parts, and we need to describe only one of them, which we denote $\mathcal{A}_5$. The integration over the whole reduced moduli space can then be written

$$\int_{\mathcal{V}_{0,5}} d\lambda_1 \wedge \ldots \wedge d\lambda_4 \langle \Sigma | b(v_{\lambda_1}) \ldots b(v_{\lambda_4}) | \Psi_1 \rangle | \Psi_2 \rangle | \Psi_3 \rangle | \Psi_4 \rangle | \Psi_5 \rangle = \tag{5.1}$$

$$= \left(\int_{\mathcal{A}_5} + \int_{\frac{1}{\mathcal{A}_5}} + \int_{1-\mathcal{A}_5} + \int_{\frac{1}{1-\mathcal{A}_5}} + \int_{1-\frac{1}{\mathcal{A}_5}} + \int_{\frac{\mathcal{A}_5}{\mathcal{A}_5-1}} \right) \Big(F(\Psi_1, \Psi_2, \Psi_3 | \Psi_4, \Psi_5) + \text{permutations} \Big) + \text{c.c.} \,,$$

where we denote

$$F(\Psi_1, \Psi_2, \Psi_3 | \Psi_4, \Psi_5) \equiv d\lambda_1 \wedge \ldots \wedge d\lambda_4 \langle \Sigma | b(v_{\lambda_1}) \ldots b(v_{\lambda_4}) | \Psi_1 \rangle | \Psi_2 \rangle | \Psi_4 \rangle | \Psi_5 \rangle | \Psi_3 \rangle \,, \tag{5.2}$$

and it is understood that the first three states are inserted on the quadrilateral faces (i.e. the punctures $z_1 = 0$, $z_2 = 1$ and $z_5 = \infty$). The integrand on the second line of (5.1) is the sum of the ten permutations of $F(\Psi_1, \Psi_2, \Psi_3 | \Psi_4, \Psi_5)$, each permutation being determined by which states are assigned to the first three arguments (i.e. the quadrilaterals faces). We are then left with six integrals that can all be written as integrals over $\mathcal{A}_5$ after pulling back their integrands through the aforementioned $\mathrm{PSL}(2,\mathbb{C})$ maps, which are explicitly

$$z \to z \,, \quad z \to \frac{1}{z} \,, \quad z \to 1 - z \,, \quad z \to \frac{1}{1-z} \,, \quad z \to 1 - \frac{1}{z} \,, \quad z \to \frac{z}{z-1} \,. \tag{5.3}$$

The six other integrals, over the complex conjugates of the six domains, can be trivially pulled back to integrals over the six domains because the transformation is simply complex conjugation. This contribution is therefore the complex conjugate in (5.1).

Now we need to describe $\mathcal{A}_5$. Let us define $\mathcal{V}_{0,5}^{\{0,1,\infty\}}$ to be the part of $\mathcal{V}_{0,5}$ whose three quadrilaterals correspond to the punctures $z = 0$, $z = 1$ and $z = \infty$. Its projection on the ξ_1-plane is shown on Figure 7. The six mappings (5.3), and complex conjugation, transform simultaneously ξ_1 and ξ_2, we could thus choose to fix either one in a given region. We choose to keep ξ_1 in the region $\mathcal{A}_5^{(1)}$, characterized by being above the real axis, on the left of the line $\mathrm{Re}\,\xi_1 = \frac{1}{2}$ and outside the unit circle centered on zero (see Figure 7); and ξ_2 is unconstrained by these mappings. So $\mathcal{A}_5^{(1)}$ is the projection of $\mathcal{A}_5$ on the ξ_1-plane.

We will now describe the remaining boundaries of $\mathcal{A}_5^{(1)}$, namely the two curves $\mathcal{B}_1$ and $\mathcal{B}_2$. In order to do this we must anticipate a little bit on the computation of the two-dimensional sections of $\mathcal{A}_5$ (the regions in the ξ_2-plane with fixed ξ_1). To make things clear, if we parameterize the four-dimensional moduli space by the four real coordinates $(\mathrm{Re}\,\xi_1, \mathrm{Im}\,\xi_1, \mathrm{Re}\,\xi_2, \mathrm{Im}\,\xi_2)$, the section S_{ξ_1} is the subset of the ξ_2-plane for which $(\mathrm{Re}\,\xi_1, \mathrm{Im}\,\xi_1, \mathrm{Re}\,\xi_2, \mathrm{Im}\,\xi_2)$ is inside the moduli space. We

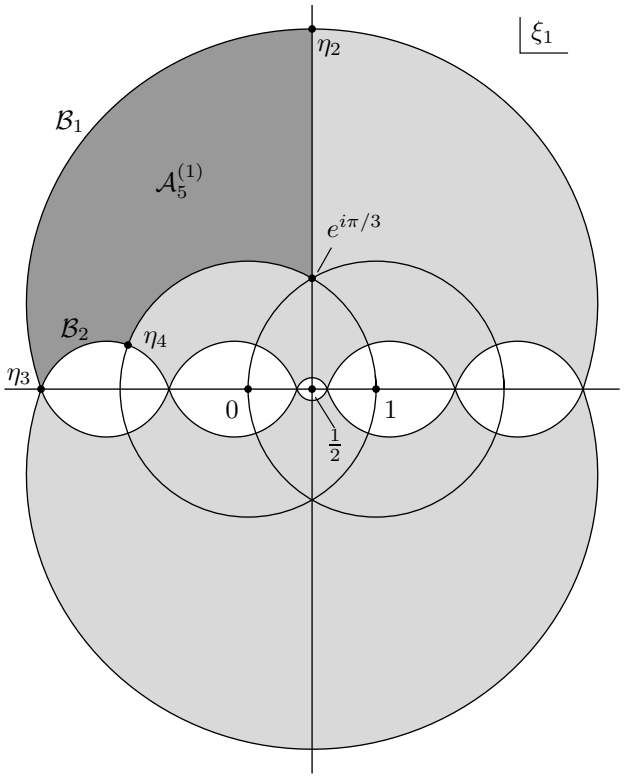

Figure 7: The projection of $\mathcal{V}_{0,5}^{\{0,1,\infty\}}$ on the ξ_1-plane. The darker region is the projection of $\mathcal{A}_5$.

present now on Figure 8, a picture of $\mathcal{A}_5$, i.e. at various points ξ_1 of $\mathcal{A}_5^{(1)}$ we show the section S_{ξ_1}. The boundaries of these sections are of two kinds, the first kind is when an edge of the prism has length π, while the boundaries of the second kind are found when an edge has vanishing length (these are drawn with a thick line on Figure 8). It is clear that when ξ_1 approaches the boundaries $\mathcal{B}_1$ or $\mathcal{B}_2$, the section S_{ξ_1} must shrink to a point. As we will see below, the sections near $\mathcal{B}_1$ have two boundaries of the second kind, so when this is reduced to a point, we must have simultaneously two edges with length zero. Near $\mathcal{B}_2$, the sections have only one boundary of the second kind, but three boundaries of the first kind. So on $\mathcal{B}_2$ we must have simultaneously one length zero and three lengths π. As can be checked on Figure 1 and Equ.(1.5) by exhaustion of all possibilities, this implies that two edges have vanishing lengths. In other words, *a sphere on the boundary $\mathcal{B}_1$ or $\mathcal{B}_2$ is described by a quadratic differential with two double zeros.* We now understand the importance of the quadratic differentials discussed in Subsection 3.2, and we are glad that they could be solved in terms of the algebraic curve $T(\ell)$ Equ.(3.36).

What we must do now is to list all the conformal and anti-conformal maps $z = h(w)$ such that the poles $\{-1, 1, \alpha, -\alpha, \infty\}$ of the quadratic differentials with two double zeros of Subsection 3.2 are mapped to the poles in the z-plane $\{0, 1, \xi_1, \xi_2, \infty\}$, and such that the critical graph (Figure 4) is mapped to a critical graph that is obtainable continuously from the graph of the right of Figure 2 by the vanishing of two lengths, and such that ξ_1 belongs to the region characterized by having

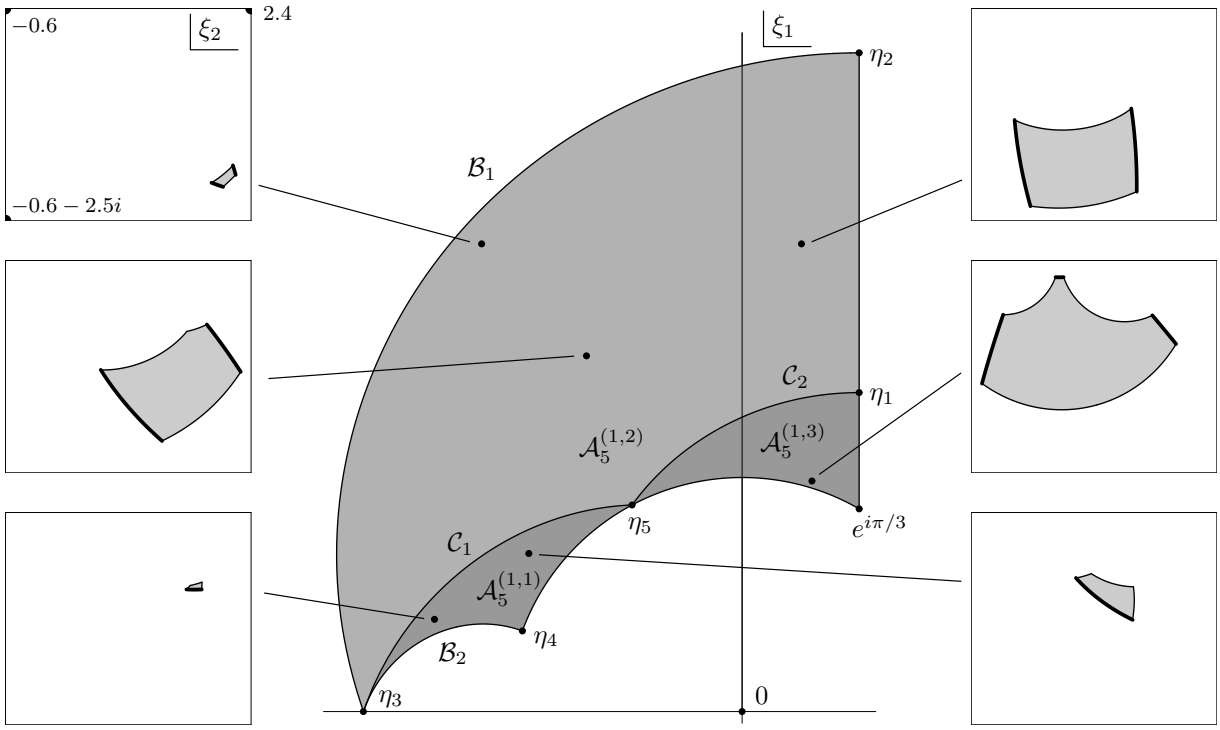

Figure 8: The projection of $\mathcal{A}_5$ on the ξ_1-plane. At various values of ξ_1, we show the section of the moduli space in the ξ_2-plane. The boxes all have the same scale. It is clearly visible that when we approach the boundaries $\mathcal{B}_1$ or $\mathcal{B}_2$, the section shrinks to zero. The thick boundaries of the sections are boundaries of the second kind, the others are of the first kind.

positive imaginary part, real part smaller that 1/2 and absolute value greater than one. There are four maps obeying all these requirements. The first one is

$$h_1(w) = \overline{\left(\frac{\alpha - w}{2\alpha}\right)}\,, \tag{5.4}$$

which maps

$$h_1(\infty) = \infty\ , \quad h_1(-\alpha) = 1\ , \quad h_1(\alpha) = 0\,, \tag{5.5}$$

and ξ_1 and ξ_2 must therefore be the images of -1 and 1.

$$\xi_1 = h_1(-1) = \overline{\left(\frac{\alpha+1}{2\alpha}\right)}\ , \quad \xi_2 = h_1(1) = \overline{\left(\frac{\alpha-1}{2\alpha}\right)} = 1 - \xi_1\,. \tag{5.6}$$

This corresponds to the curve $\mathcal{B}_1$

$$\boxed{\mathcal{B}_1 = \left\{ \overline{\left(\frac{\alpha(\ell)+1}{2\alpha(\ell)}\right)}\ ,\ \ell \in \left[0, \frac{\pi}{2}\right] \right\}}, \tag{5.7}$$

where $\alpha(\ell)$ is given by (3.37). The second map is

$$h_2(w) = \frac{\alpha - 1}{\alpha + 1}\frac{w-1}{w+1}\,. \tag{5.8}$$

It maps

$$h_2(1) = 0\,, \quad h_2(-1) = \infty\,, \quad h_2(-\alpha) = 1\,,$$
$$\xi_1 = h_2(\infty) = \frac{\alpha - 1}{\alpha + 1}\,, \quad \xi_2 = h_2(\alpha) = \xi_1^2\,. \tag{5.9}$$

This defines the curve $\mathcal{B}_2$

$$\boxed{\mathcal{B}_2 = \left\{ \frac{\alpha(\ell) - 1}{\alpha(\ell) + 1}\,,\ \ell \in \left[0, \frac{\pi}{2}\right] \right\}}. \tag{5.10}$$

The third map is

$$h_3(w) = \frac{2}{\alpha + 1} \frac{w - \alpha}{w - 1}\,, \tag{5.11}$$

for which

$$h_3(1) = \infty\,, \quad h_3(-1) = 1\,, \quad h_3(\alpha) = 0$$
$$\xi_1 = h_3(-\alpha) = \frac{4\alpha}{(\alpha + 1)^2}\,, \quad \xi_2 = h_3(\infty) = \frac{2}{\alpha + 1}\,. \tag{5.12}$$

We will call the corresponding curve $\mathcal{C}$

$$\mathcal{C} = \left\{ \frac{4\alpha(\ell)}{(\alpha(\ell) + 1)^2}\,,\ \ell \in \left[0, \frac{\pi}{2}\right] \right\}. \tag{5.13}$$

Before we discuss the fourth map and the meaning of the third one, we need to look at what we have found so far. At the special point $\ell = 0$, we recall (3.38) that $\alpha(0) = 2 - \sqrt{5}$ and thus we find that all three curves meet at the point η_3 (Figure 8), where

$$\eta_3 = \mathcal{B}_1|_{\ell=0} = \mathcal{B}_2|_{\ell=0} = \mathcal{C}|_{\ell=0} = -\frac{1 + \sqrt{5}}{2}\,. \tag{5.14}$$

When $\ell = \frac{\pi}{2}$, the curve $\mathcal{B}_1$ meets the axis $\mathrm{Re}\,\xi_1 = \frac{1}{2}$ at the point η_2. From (3.38) we find

$$\eta_2 = \frac{1}{2} + \frac{32\sqrt{6} + 19\sqrt{15}}{54}\, i\,. \tag{5.15}$$

Also when $\ell = \frac{\pi}{2}$, the curve $\mathcal{B}_2$ meets the unit circle at the point η_4, given by

$$\eta_4 = \frac{27 + \left(32\sqrt{6} + 19\sqrt{15}\right)\, i}{27 - \left(32\sqrt{6} + 19\sqrt{15}\right)\, i}\,. \tag{5.16}$$

The situation for the curve $\mathcal{C}$ is a little bit different because for $\ell > \ell_0 \approx 0.67622$, the curve is outside of the allowed domain because it is inside the unit circle centered at the origin. But we can map the piece of curve with $\ell > \ell_0$ back inside the domain by the map $z \to 1/\bar{z}$. So the curve $\mathcal{C}$ gives us actually two curves $\mathcal{C}_1$ and $\mathcal{C}_2$ (and the fourth map is just $h_4(w) = 1/\overline{h_3(w)}$). We have thus

$$\mathcal{C}_1 = \left\{ \frac{4\alpha(\ell)}{(\alpha(\ell) + 1)^2}\,,\ \ell \in [0, \ell_0] \right\} \quad , \qquad \mathcal{C}_2 = \left\{ \overline{\left(\frac{(\alpha(\ell) + 1)^2}{4\alpha(\ell)} \right)}\,,\ \ell \in \left[\ell_0, \frac{\pi}{2}\right] \right\}. \tag{5.17}$$

At $\ell = \ell_0$ these two curves intersect on the unit circle at the point

$$\eta_5 \approx -0.47019 + 0.88256\, i\,. \tag{5.18}$$

At last, when $\ell = \frac{\pi}{2}$, the curve $\mathcal{C}_2$ meets the axis $\mathrm{Re}\,\xi_1 = \frac{1}{2}$ at the point η_1, with

$$\eta_1 = \frac{1}{2} + \frac{19\sqrt{15}}{54}\, i\,. \tag{5.19}$$

In Figure 9 we show the critical graphs of the quadratic differentials obtained by mapping the

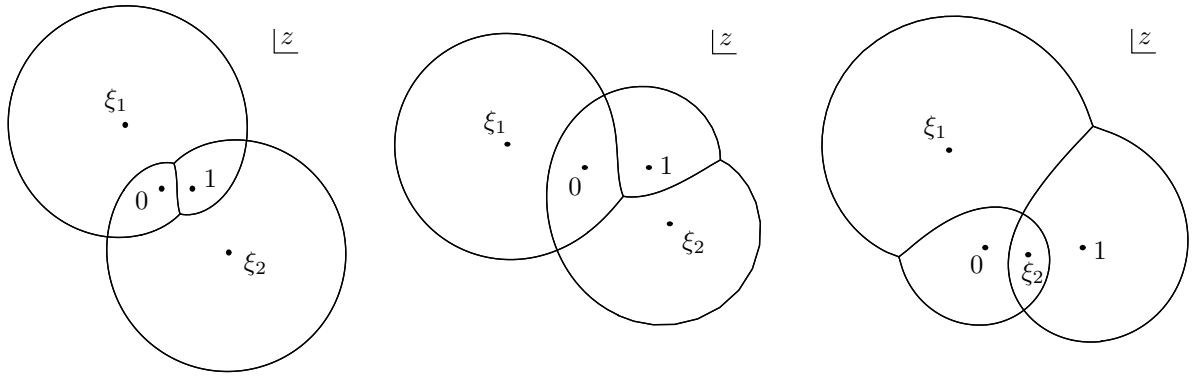

Figure 9: The critical graphs of the quadratic differentials obtained by mapping the quadratic differential of Figure 4 with, respectively, h_1, h_2 and h_3.

quadratic differential of Figure 4 with, respectively, h_1, h_2 and h_3. So they are respectively on $\mathcal{B}_1$, $\mathcal{B}_2$, and $\mathcal{C}_2$.

It remains now to understand the meaning of the curves $\mathcal{C}_1$ and $\mathcal{C}_2$. From Figure 9 we can be more specific by noting that on these curves, one quadrilateral and one triangle edge are zero. By exhausting all combinations on the prism of Figure 1 and Equ.(1.5), we see that this implies that we have also three triangle edges of length π. We thus have an intersection of three boundaries of the first kind and one boundary of the second kind. This can happen if a boundary of the second kind of the section S_{ξ_1} is reduced to a point. Therefore the curves $\mathcal{C}_1$ and $\mathcal{C}_2$ partition $\mathcal{A}_5^{(1)}$ into three regions $\mathcal{A}_5^{(1,n)}$, $n = 1, 2, 3$ in which the sections S_{ξ_1} have exactly n boundaries of the second kind. This partition is shown on Figure 8, where we can also verify the number of boundaries of the sections shown in the boxes. We do not prove that this partitioning is as shown, but we have checked it numerically beyond doubt.

To end this section, we briefly sketch how we plot numerically the sections. We start by plotting the boundaries of the second kind; this is done with the quadratic differentials with one double zero, studied in Subsection 3.1. The end of the boundaries are detected when a length is π, and accurately determined. We then start from one end (where, say, $\ell_i = 0$) to plot a boundary of the first kind by finding the points ξ_2 for which $\ell_i = \pi$. We end either when another length (say ℓ_j) becomes π, or when we end up very close to a boundary of the second kind. In the first case, we

determine accurately the corner (the intersection of two boundaries) and continue by looking at the points for which $\ell_j = \pi$. In the second case we go on by plotting the boundary of the first kind attached to the other end of the boundary of the second kind that we just met. We continue this process until we arrive at the other end of the second-kind boundary from which we started. The result will be a closed curve given by a set of points separated by an approximately fixed distance h; and the special points at the corners of the curve are always precisely given.

6 The five-tachyon contact term

To calculate the five-tachyon contact term, we take the general formula established in [9] for the N-tachyon term (or use Equ.(7.25)). Namely

$$\kappa^2 V_{t^N} = \frac{(-1)^{N-1}}{N!} \frac{2}{\pi^{N-3}} \int_{\mathcal{V}_{0,N}} \prod_{i=1}^{N-3} \frac{dx_i \wedge dy_i}{\rho_i^2} \frac{1}{\rho_{N-2}^2(0)\rho_{N-1}^2(1)\rho_N^2(\infty)} \tag{6.1}$$

where $\xi_i = x_i + i\, y_i$. Since the five external states are the same, the integration over $\mathcal{V}_{0,5}$ can be written as 120 times the integration over $\mathcal{A}_5$. Therefore

$$\kappa^2 V_{t^5} = \frac{2}{\pi^2} \int_{\mathcal{A}_5} dx_1 \wedge dy_1 \wedge dx_2 \wedge dy_2\, \mu(\xi_1, \bar{\xi_1}, \xi_2, \bar{\xi_2}) \quad , \qquad \mu \equiv \frac{1}{(\rho_1\rho_2\rho_3\rho_4\rho_5)^2}\,, \tag{6.2}$$

It is now a good place to explain how we perform the numerical integration. There are five distinct steps in the process.

Step 1 First we compute the boundary of the reduced moduli space. For this we draw a covering rectangular grid of $(N+1) \times (N+1)$ points on $\mathcal{A}_5^{(1)}$, the projection of $\mathcal{A}_5$ on the ξ_1-plane. Then at each of the points ξ_1 of the grid we *attempt* to plot, in the ξ_2-plane, the boundary of the section S_{ξ_1}. In the ξ_2-plane, this boundary is represented as a list of points, and the space between two successive points is taken to be approximately h. It may happen that the algorithm fails to find a Strebel differential because the Newton method fails to converge (for example if we are close to a singular quadratic differential, near the boundaries $\mathcal{B}_1$ or $\mathcal{B}_2$). In that case, the algorithm may be able to fix the problem by trying other initial values; if this still fails the consequence may be that the algorithm is unable to draw the section, but this is not dramatic, it simply keeps record of this failure and proceeds to the next point of the grid. We are using three different grids which have respectively $(N, h) = (30, 0.1)$, $(70, 0.05)$ and $(100, 0.03)$. On Figure 10 we show all the points of these three grids for which the section could be plotted. We see that we have some gaps near the boundary $\mathcal{B}_1$, especially near the point η_3 where it meets the boundary $\mathcal{B}_2$. This is not surprising because at this point the quadratic differential has two triple zeros, a very singular point indeed. But it is clear that as we increase the number of points on the grid, the gaps are becoming smaller. This is due to the fact that, going from one point to the next, the quadratic differential solver based on the Newton method, can use the solutions of the nearby points as seeds, and of course if they are closer the Newton method will have more chance to converge. The grid with $N = 100$ is however already at the limit of the computational power of a desktop computer. We notice also a few gaps

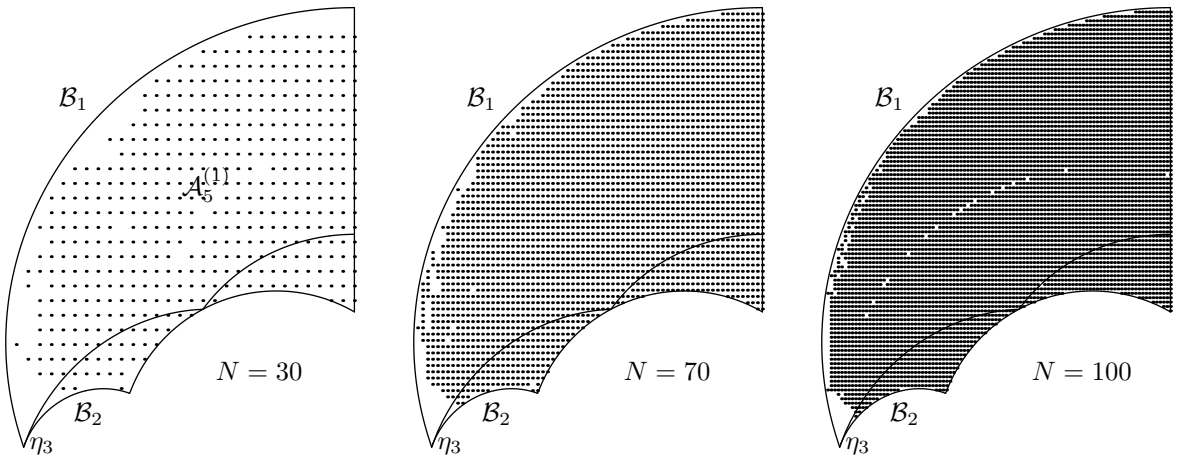

Figure 10: The projection of $\mathcal{A}_5$ covered with grids of $(N+1)\times(N+1)$ points with $N = 30$, 70 and 100. The dots represent the points of the grids for which the section could be computed.

away from the boundaries, and most noticeably there seems to be a line of gaps in the middle of the grid $N = 100$. The failure there is actually not due to the Newton method but to the difficulty of plotting the boundary of a section when one very small boundary of the first kind is stuck between two other boundaries of the first kind. This could be fixed by improving the algorithm, but we don't really need to do this at this point because we will eventually use quadratic interpolation to fix these gaps. One may worry about the size of the gaps near $\mathcal{B}_1$ and especially near $\xi_1 = \eta_3$, but we recall that near the boundaries $\mathcal{B}_1$ and $\mathcal{B}_2$ the sections become small, and therefore the gaps actually represent a small four-dimensional volume, and will be fixed by extrapolation. The error made by the interpolations and extrapolation will be estimated later.

Step 2 Now we cover every section with a rectangular grid, with spacing s along the real and imaginary directions, and at every of these points we attempt to find the Strebel quadratic differential. Again it is possible that some differentials are not found, but this will be fixed by interpolation (extrapolation). At every of these points, we store all the data of the quadratic differential, i.e. ξ_i, a_i, $\partial a_i/\partial\xi_j$, $\partial a_i/\partial\bar{\xi_j}$, $i,j = 1,2$ and ρ_I, $I = 1,\ldots,5$. For our three particular grids $N = 30$, 70 and 100, the spacing s is chosen as respectively $s = 0.1$, 0.05 and 0.04. We also consider the same grid $N = 70$ with the smaller spacing $s = 0.04$.

Step 3 We integrate μ on every sections.

$$M(\xi_1,\bar{\xi_1}) \equiv \int_{S_{\xi_1}} dx_2 \wedge dy_2\, \mu(\xi_1,\bar{\xi_1},\xi_2,\bar{\xi_2}) \quad , \quad \xi_2 = x_2 + i\, y_2\,. \tag{6.3}$$

because the shapes of the sections are complicated, we use a Monte-Carlo technique and integrate the function

$$\mu'(\xi_1,\bar{\xi_1},\xi_2,\bar{\xi_2}) = \begin{cases} \mu(\xi_1,\bar{\xi_1},\xi_2,\bar{\xi_2}) & \text{if} \quad \xi_2 \in S_{\xi_1} \\ 0 \quad \text{otherwise} \end{cases} \tag{6.4}$$

over a rectangle containing the section S_{ξ_1}. To evaluate μ at random points ξ_2 we use quadratic interpolation over the closest 3×3 sub-array of points of the grid. Actually, we find it more natural to interpolate $\log\mu$, and exponentiate the result of the interpolation.

Step 4 We can finally perform the whole integration

$$\int_{\mathcal{A}_5} dx_1\wedge dy_1\wedge dx_2\wedge dy_2\,\mu(\xi_1,\bar{\xi_1},\xi_2,\bar{\xi_2}) = \int_{\mathcal{A}_5^{(1)}} dx_1\wedge dy_1\,M(\xi_1,\bar{\xi_1})\,. \tag{6.5}$$

We use again a Monte-Carlo technique, integrating

$$M'(\xi_1,\bar{\xi_1}) = \begin{cases} M(\xi_1,\bar{\xi_1}) & \text{if} \quad \xi_1\in\mathcal{A}_5^{(1)} \\ 0 \quad \text{otherwise} \end{cases}\quad, \tag{6.6}$$

and integrate M' over a rectangle containing $\mathcal{A}_5^{(1)}$. To evaluate M, we use again quadratic interpolation of $\log M$, and exponentiate the result of the interpolation; we observe that it is a better interpolation that if we had simply interpolated M itself.

Step 5: Error estimation We would like to calculate an estimate of the numerical uncertainty on the result. There are four sources of error, namely

1. The error due to the finite spacing h. In order to decide if $\xi_2\in S_{\xi_1}$, we check if ξ_2 is inside the polygon formed by all points describing the boundary of S_{ξ_1}. This is basically a linear interpolation, so the error made will be of the order of h^2, a potentially large error. To reduce it, we are computing the integral twice, once in the normal way, and a second time with all the sections replaced with cruder ones with spacing $2h$. Practically we are removing half the points of every sections but keep the corners (the intersections between boundaries). In order to isolate this source of errors from the other sources, it is important to use the same Monte-Carlo samples in both integrations (i.e. the sequence of random points must be the same). Let us denote $\kappa^2 V_{t^5}(h)$ and $\kappa^2 V_{t^5}(2h)$ the results of these two integrations, and let $\kappa^2 V_{t^5}$ be the exact value. Since the error is quadratic in h, we have

$$\kappa^2 V_{t^5}(2h) - \kappa^2 V_{t^5} = 4\left(\kappa^2 V_{t^5}(h) - \kappa^2 V_{t^5}\right) + \mathcal{O}(h^3)\,, \tag{6.7}$$

   or in other words

$$\kappa^2 V_{t^5} = \frac{1}{3}\left(4\kappa^2 V_{t^5}(h) - \kappa^2 V_{t^5}(2h)\right) + \mathcal{O}(h^3)\,, \tag{6.8}$$

   and it will turn out that we can neglect the residual error as it will be smaller than the other sources.

2. The error done by the interpolation and extrapolation of μ. Let us write $\mu = \mu_{\text{inter}} + \delta_\mu$. We will then treat this source of error as systematic, in other words

$$\sigma_2 \equiv \int_{\mathcal{A}_5} dx_1\wedge dy_1\wedge dx_2\wedge dy_2\,\left|\delta_\mu(\xi_1,\bar{\xi_1},\xi_2,\bar{\xi_2})\right|\,. \tag{6.9}$$

   The quadratic interpolation is done with the routine `polin2` of [18]. Based on Neville's algorithm, it can give an estimate of $\delta_\mu(\xi_1,\bar{\xi_1},\xi_2,\bar{\xi_2})$.

3. the error due to the interpolation and extrapolation of M. It is a systematic error as well. We write $M = M_{\text{inter}} + \delta_M$ and

$$\sigma_3 \equiv \int_{\mathcal{A}_5^{(1)}} dx_1 \wedge dy_1 \; |\delta_M| \tag{6.10}$$

4. The error coming from the Monte-Carlo integrations. Those are purely statistical errors, and the errors coming from the integrations in Step 3 will cancel down to a negligible quantity in the final result if they are done with enough samples. We are thus only considering the Monte-Carlo error σ_{MC} on the last integral of Step 4.

So finally

$$\sigma^2_{\kappa^2 V_{t^5}} = \frac{2}{\pi^2} \left(\sigma_2^2 + \sigma_3^2 + \sigma_{MC}^2 \right) , \tag{6.11}$$

and we will take enough samples in the Monte-Carlo integration so that the error will be dominated by the errors on interpolation and extrapolation, which depend on the finesse of the grid.

We note that Steps 1 and 2 need to be done only once for every grid. Once these have been done, every integration requires only Steps 3, 4 and 5.

We now state our results. We use four different grids, with (N, h, s) respectively equal to $(30, 0.1, 0.1)$, $(70, 0.05, 0.05)$, $(70, 0.05, 0.04)$ and $(100, 0.03, 0.04)$. These last two grids are at the computational limit of a desktop computer with our C++ code. Indeed it takes several days to compute $a_i(\xi_1, \bar{\xi_1}, \xi_2, \bar{\xi_2})$ and their derivatives and $\rho_I(\xi_1, \bar{\xi_1}, \xi_2, \bar{\xi_2})$ at every points of the four-dimensional grid $(70, 0.05, 0.04)$ (which has approximately 1.6 million points inside $\mathcal{A}_5$, and fills 1.3 GBytes of RAM). The grid $(100, 0.03, 0.04)$ is actually too large to store the derivatives of a_i, so we can use it only for the computation of $\kappa^2 V_{t^5}$. The computation of the five-dilaton contact term in Section 7 will have to be done with the grid $(70, 0.05, 0.04)$. All the Monte-Carlo integrations are done with one iteration of the routine `vegas` of [18]. The integrations of Step 3 are done with 10^5 samples, and the integrations of Step 4 are done with 10^6 samples. Our results are shown in Table 1. It is reassuring that all four results are compatible within their error bounds. They are

(N, h, s)	$(30, 0.1, 0.1)$	$(70, 0.05, 0.05)$	$(70, 0.05, 0.04)$	$(100, 0.03, 0.04)$
$\kappa^2 V_{t^5}(2h)$	10.0774 ± 0.065	9.95537 ± 0.013	9.95197 ± 0.010	9.93412 ± 0.008
$\kappa^2 V_{t^5}(h)$	10.0045 ± 0.065	9.93535 ± 0.013	9.93252 ± 0.010	9.92648 ± 0.008
$\kappa^2 V_{t^5}$	9.980 ± 0.065	9.929 ± 0.013	9.926 ± 0.010	9.924 ± 0.008

Table 1: The results of the integrations and their uncertainties on our three different grids.

not statistically independent however, and we should therefore not combine them. So we take the result from the finest grid as final answer

$$\boxed{\kappa^2 V_{t^5} = 9.924 \pm 0.008} . \tag{6.12}$$

7 The five-dilaton effective term

The goal of this section is to check the validity of our computation. The quartic vertex computed in [7] was checked in [10] with marginal fields. A similar analysis is unfortunately not possible here because we can couple only an even number of marginal fields like $\alpha_{-1}\bar{\alpha}_{-1}c_1\bar{c}_1|0\rangle$ and the vanishing of the quintic term of its effective potential is trivial. However we can compute the amplitude of five dilatons $|D\rangle$, where

$$|D\rangle = (c_1 c_{-1} - \bar{c}_1\bar{c}_{-1})\,|0\rangle\,, \tag{7.1}$$

and compare it to the prediction of the dilaton theorem.

The dilaton theorem states that the effective potential of the dilaton should be identically zero. That the $V^{\text{eff}}_{d^3}$ term vanishes is due to the fact that the cubic amplitude of three dilatons is zero because the ghost numbers do not work out. The vanishing of $V^{\text{eff}}_{d^4}$ is nontrivial; it has been checked in [11] that the contribution from the quartic amplitude $\kappa^2 V_{d^4}$ cancels the contribution from Feynman diagrams with two cubic vertices. This cancellation was found to be good to about 0.2%, furnishing a very good evidence that the quartic computations are done right. In this section, we want to check the vanishing of $V^{\text{eff}}_{d^5}$. There are two contributions to this effective term shown on Figure 11, namely the contact term $\kappa^2 V_{d^5}$, and the Feynman term $\mathcal{C}_{d^5}$

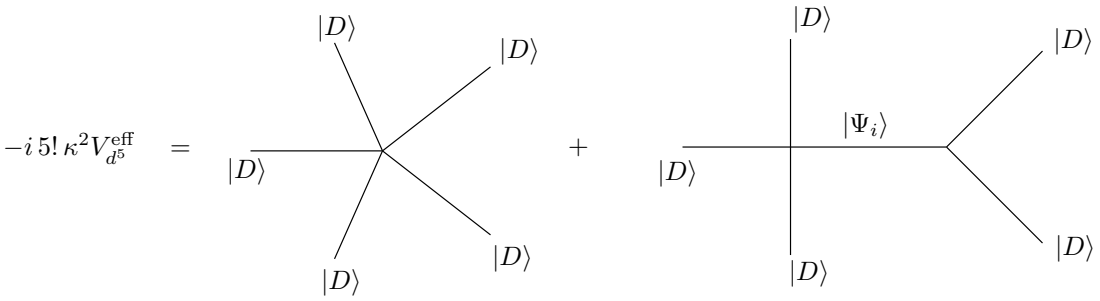

Figure 11: The term d^5 of the dilaton effective potential. The fields $|\Psi_i\rangle$ that propagate in the second diagram, are the tachyon and all the massive fields, but not the dilaton.

$$\kappa^2 V^{\text{eff}}_{d^5} = \kappa^2 V_{d^5} + \mathcal{C}_{d^5}\,. \tag{7.2}$$

We will start by evaluating the Feynman contribution, then we will compute the contact term with the machinery developed in this paper.

7.1 The Feynman contribution

The three-string vertex can couple only an even number of states with asymmetric ghost numbers like the dilaton. So the diagram consisting of three three-string vertices doesn't contribute, and the only Feynman diagram contributing to $\mathcal{C}_{d^5}$ is therefore the one shown on the right of Figure 11. To get the right relative sign between this diagram and the contact term, we must keep track

of all the coefficients. Since the vertices bring in the amplitude a factor $-i$, and the propagator a factor i, we have

$$\begin{aligned}(-i)\,5!\,\mathcal{C}_{d^5} &= \binom{5}{3}\sum_{i,j\neq 2}(-i)\,\{D,D,D,\Psi_i\}\,(i)\,\left(-M^{-1}\right)_{ij}(-i)\,\{D,D,\Psi_j\}\,,\\ \Rightarrow \mathcal{C}_{d^5} &= -\frac{1}{12}\sum_{i,j\neq 2}\{D,D,D,\Psi_i\}\left(M^{-1}\right)_{ij}\{D,D,\Psi_j\}\,,\end{aligned} \tag{7.3}$$

where $(-M^{-1})$ is the zero-momentum propagator for all the fields except the dilaton. M is therefore given by the quadratic term

$$M_{ij} = \langle\Psi_i|c_0^- Q_B|\Psi_j\rangle\,,\quad i,j\neq 2\,. \tag{7.4}$$

Note that we work in a non-orthonormal basis, and M is therefore not diagonal. $\mathcal{C}_{d^5}$ must be evaluated with level truncation, we will do explicitly the first few levels. First it is convenient to decompose $\mathcal{C}_{d^5}$ into the sum of contributions at every level

$$\mathcal{C}_{d^5}(\ell) = \sum_{\ell'\leq\ell} c_{d^5}(\ell')\,. \tag{7.5}$$

And we will write M_ℓ for the matrix M with only fields of level ℓ, and we define the row vectors

$$\begin{aligned}C_\ell &\equiv (\{D,D,\Psi_i\})\\ Q_\ell &\equiv (\{D,D,D,\Psi_i\})\,,\end{aligned} \tag{7.6}$$

where the index i runs over all fields of level ℓ. With these notations, we can write

$$c_{d^5}(\ell) = -\frac{1}{12}Q_\ell\cdot M_\ell^{-1}\cdot C_\ell^T\,. \tag{7.7}$$

At level zero, only the tachyon propagates, and we thus have

$$\mathcal{C}_{d^5}(0) = -\frac{1}{12}\{D,D,D,T\}\,M_0^{-1}\,\{D,D,T\} = -\frac{1}{12}(-5.716)(-\frac{1}{2})(-\frac{27}{16}) = 0.4020\,. \tag{7.8}$$

At level four, the four fields are (we are using the notations of [15])

$$\begin{aligned}|\Psi_3\rangle &= \left(b_{-2}c_1\bar{c}_{-2}\bar{c}_1 - \bar{b}_{-2}\bar{c}_1 c_{-2}c_1\right)|0\rangle\,,\quad |\Psi_4\rangle = c_{-1}\bar{c}_{-1}|0\rangle\\ |\Psi_5\rangle &= L_{-2}c_1\bar{L}_{-2}\bar{c}_1|0\rangle\,,\quad |\Psi_6\rangle = \left(c_{-1}\bar{L}_{-2}\bar{c}_1 - \bar{c}_{-1}L_{-2}c_1\right)|0\rangle\,.\end{aligned} \tag{7.9}$$

And we have

$$\begin{aligned}M_4 &= \mathrm{diag}\,(-4,2,338,-52)\\ C_4 &= \left(0,-\frac{1}{48},-\frac{4225}{432},\frac{65}{72}\right)\\ Q_4 &= (-4.547,-1.811,-22.33,10.69)\end{aligned} \tag{7.10}$$

The first two lines are done with standard techniques, and the third line has been calculated in [15], we refer the reader to [15] and [11] for the details of this computation. With these values (7.7) gives the contribution of level four

$$c_{d^5}(4) = -0.03996 \tag{7.11}$$

which gives the total contribution

$$\mathcal{C}_{d^5}(4) = \mathcal{C}_{d^5}(0) + c_{d^5}(4) = 0.3620\,. \tag{7.12}$$

At level six, the fields are

$$\begin{aligned}
&|\Psi_7\rangle = \left(b_{-2}\bar{c}_{-2}\bar{c}_{-1}\bar{c}_1 - \bar{b}_{-2}c_{-2}c_{-1}c_1\right)|0\rangle\ , \quad |\Psi_8\rangle = \left(L_{-2}\bar{c}_{-3}\bar{c}_1 - \bar{L}_{-2}c_{-3}c_1\right)|0\rangle \\
&|\Psi_9\rangle = L_{-2}\bar{L}_{-2}\left(\bar{c}_{-1}\bar{c}_1 - c_{-1}c_1\right)|0\rangle\ , \quad |\Psi_{10}\rangle = \left(b_{-3}c_1\bar{c}_{-3}\bar{c}_1 - \bar{b}_{-3}\bar{c}_1c_{-3}c_1\right)|0\rangle \\
&|\Psi_{11}\rangle = \left(b_{-3}c_1\bar{L}_{-2}\bar{c}_{-1}\bar{c}_1 - \bar{b}_{-3}\bar{c}_1L_{-2}c_{-1}c_1\right)|0\rangle\ , \quad |\Psi_{12}\rangle = c_{-2}\bar{c}_{-2}|0\rangle\ , \quad |\Psi_{13}\rangle = L_{-3}c_1\bar{L}_{-3}\bar{c}_1|0\rangle \\
&|\Psi_{14}\rangle = b_{-2}c_{-1}c_1\bar{b}_{-2}\bar{c}_{-1}\bar{c}_1|0\rangle\ , \quad |\Psi_{15}\rangle = \left(c_{-2}\bar{L}_{-3}\bar{c}_1 - \bar{c}_{-2}L_{-3}c_1\right)|0\rangle \\
&|\Psi_{16}\rangle = \left(c_{-2}\bar{b}_{-2}\bar{c}_{-1}\bar{c}_1 - \bar{c}_{-2}b_{-2}c_{-1}c_1\right)|0\rangle\ , \quad |\Psi_{17}\rangle = \left(L_{-3}c_1\bar{b}_{-2}\bar{c}_{-1}\bar{c}_1 - \bar{L}_{-3}\bar{c}_1b_{-2}c_{-1}c_1\right)|0\rangle\,,
\end{aligned}$$

and we have

$$\begin{aligned}
M_6 &= \begin{pmatrix} 8 \end{pmatrix} \oplus \begin{pmatrix} 0 & 0 & 0 & -104 \\ 0 & -1352 & 0 & 0 \\ 0 & 0 & -8 & 0 \\ -104 & 0 & 0 & 0 \end{pmatrix} \oplus \begin{pmatrix} 0 & 0 & 4 \\ 0 & 10816 & 0 \\ 4 & 0 & 0 \end{pmatrix} \oplus \begin{pmatrix} 0 & 0 & 416 \\ 0 & 8 & 0 \\ 416 & 0 & 0 \end{pmatrix} \\
C_6 &= \frac{100}{729}\,(-8,0,0,0,0,1,0,4,0,4,0) \\
Q_6 &= (-2.103, 2.363, -20.92, -0.4412, 7.090, 0.1251, -49.67, 0.4998, 4.325, 1.603, -8.649)\ .
\end{aligned} \tag{7.13}$$

And we find

$$c_{d^5}(6) = -0.03606\,, \tag{7.14}$$

which gives the total contribution

$$\mathcal{C}_{d^5}(6) = \mathcal{C}_{d^5}(4) + c_{d^5}(6) = 0.3259\,. \tag{7.15}$$

With the techniques developed in [7, 12, 11, 10, 15], we can evaluate $\{D, D, D, \Psi_i\}$ for fields Ψ_i of level up to ten. The results for $\mathcal{C}_{d^5}(\ell)$, $\ell = 0, 4, 6, 8, 10$ are shown in Table 2. We will follow the

ℓ	0	4	6	8	10
$\mathcal{C}_{d^5}(\ell)$	0.4020	0.3620	0.3259	0.3167	0.3112

Table 2: The value of $\mathcal{C}_{d^5}$ with propagating fields up to level ℓ.

method used in [11] to extrapolate the above results to $\ell = \infty$. Namely we use a fit of the form

$$\mathcal{C}_{d^5}(\ell) = f_0 + \frac{f_1}{\ell^\gamma}\,. \tag{7.16}$$

In fitting $\mathcal{C}_{d^4}(\ell)$, the authors of [11] found that $\gamma = 3$ give the best results. Here by fitting the four values $\mathcal{C}_{d^5}(\ell)$, $\ell = 4, 6, 8, 10$ with (7.16), we find that $\gamma = 2.51$. We take this as an evidence that the data should be fitted with

$$\mathcal{C}_{d^5}(\ell) = f_0 + \frac{f_1}{\ell^{5/2}}\,. \tag{7.17}$$

With this last fit we find

$$\boxed{\mathcal{C}_{d^5} = \mathcal{C}_{d^5}(\infty) = 0.3060}\,. \tag{7.18}$$

7.2 The contact term

The multilinear N-string function at genus zero is given by [1, 9]

$$\{\Psi_1, \ldots, \Psi_N\} = \left(\frac{i}{2\pi}\right)^{N-3} \int_{\mathcal{V}_{0,N}} d\lambda_1 \wedge \ldots \wedge d\lambda_{2(N-3)} \langle \Sigma | b(v_{\lambda_1}) \ldots b(v_{\lambda_{2(N-3)}}) | \Psi_1 \rangle \ldots | \Psi_N \rangle\,. \tag{7.19}$$

The λ_i are $2(N-3)$ real coordinates of the reduced moduli space $\mathcal{V}_{0,N}$ of the N-punctured spheres, and the surface state $\langle \Sigma|$ corresponds to the N-punctured sphere given by the parameters λ_i. The antighost insertions $b(v_{\lambda_i})$ are given by

$$b(v_{\lambda_i}) = \sum_{I=1}^{N} \sum_{m=-1}^{\infty} \left(H^I_{i,m} b^{(I)}_m + \overline{H^I_{i,m}} \bar{b}^{(I)}_m \right)\,, \quad \text{where} \quad H^I_{i,m} = \oint \frac{dw}{2\pi i} \frac{1}{w^{m+2}} \frac{1}{h'_I} \frac{\partial h_I}{\partial \lambda_i}\,. \tag{7.20}$$

The $h_I(w_I; \lambda_1, \ldots \lambda_{2(N-3)})$ are the N maps from the local coordinates w_I to the sphere, which are going to be described a little later. Now we follow [11] and rewrite the antighost insertions in a more convenient form. First we rename the coordinates of the moduli space as

$$\xi_i = x_i + i\, y_i\,, \quad \text{where} \quad x_i = \lambda_{2i-1}\,,\ y_i = \lambda_{2i}\,,\ i = 1, \ldots, N-3\,, \tag{7.21}$$

where the ξ_i are the complex coordinates naturally used in the quadratic differentials formalism. We have

$$dx_i \wedge dy_i\, b(v_{x_i}) b(v_{y_i}) = d\xi \wedge d\bar{\xi}\, \mathcal{B}_i \mathcal{B}^\star_i = -2i\, dx_i \wedge dy_i\, \mathcal{B}_i \mathcal{B}^\star_i\,, \tag{7.22}$$

where

$$\mathcal{B}_i = \sum_{I=1}^{N} \sum_{m=-1}^{\infty} \left(B^I_{i,m} b^{(I)}_m + \overline{C^I_{i,m}} \bar{b}^{(I)}_m \right) \quad , \quad \mathcal{B}^\star_i = \sum_{I=1}^{N} \sum_{m=-1}^{\infty} \left(C^I_{i,m} b^{(I)}_m + \overline{B^I_{i,m}} \bar{b}^{(I)}_m \right)\,, \tag{7.23}$$

and the coefficients $B^I_{i,m}$ and $C^I_{i,m}$ are given in terms of derivatives with respect to ξ_i and $\bar{\xi}_i$

$$B^I_{i,m} = \oint \frac{dw}{2\pi i} \frac{1}{w^{m+2}} \frac{1}{h'_I} \frac{\partial h_I}{\partial \xi_i} \quad , \quad C^I_{i,m} = \oint \frac{dw}{2\pi i} \frac{1}{w^{m+2}} \frac{1}{h'_I} \frac{\partial h_I}{\partial \bar{\xi}_i}\,. \tag{7.24}$$

And we arrive at the formula

$$\{\Psi_1, \ldots, \Psi_N\} = \frac{1}{\pi^{N-3}} \int_{\mathcal{V}_{0,N}} dx_1 \wedge dy_1 \wedge \ldots \wedge dx_{N-3} \wedge dy_{N-3} \langle \Sigma | \left(\mathcal{B}\mathcal{B}^\star\right)_1 \ldots \left(\mathcal{B}\mathcal{B}^\star\right)_{N-3} | \Psi_1 \rangle \ldots | \Psi_N \rangle\,. \tag{7.25}$$

We will now consider the case of interest, $N = 5$ and $|\Psi_i\rangle = |D\rangle$, where $|D\rangle$ is the dilaton (7.1). we will thus only need the coefficients $B^I_{i,m}$ and $C^I_{i,m}$ with $m = -1$ and $m = 1$. To evaluate them, we need to expand the maps h_I to order w^3

$$z = h_I(w_I; \xi_1, \bar{\xi_1}, \xi_2, \bar{\xi_2}) = z_I + \rho_I\, w_I + \rho_I^2 \beta_I\, w_I^2 + \rho_I^3 \gamma_I\, w_I^3 + \mathcal{O}(w_I^4)\,, \tag{7.26}$$

where all the coefficients on the right-hand side depend on ξ_1, $\bar{\xi_1}$, ξ_2 and $\bar{\xi_2}$. The z_I are the positions of the finite poles on the z-plane, namely

$$z_1 = 0 \quad , \quad z_2 = 1 \quad , \quad z_3 = \xi_1 \quad , \quad z_4 = \xi_2\,. \tag{7.27}$$

For the puncture at infinity, we must use the coordinate $t = 1/z$

$$t = h_5(w_5; \xi_1, \bar{\xi_1}, \xi_2, \bar{\xi_2}) = \rho_5\, w_5 + \rho_5^2 \beta_5\, w_5^2 + \rho_5^3 \gamma_5\, w_5^3 + \mathcal{O}(w_5^4)\,. \tag{7.28}$$

We can now use (7.24) to express the coefficients that we need. We find

$$\begin{aligned} &B^I_{1,-1} = \frac{1}{\rho_3}\delta_{3,I} \quad , \quad B^I_{2,-1} = \frac{1}{\rho_4}\delta_{4,I} \quad , \quad C^I_{i,-1} = 0 \\ &B^I_{1,1} = \rho_I \frac{\partial \beta_I}{\partial \xi_1} + \frac{1}{2}\rho_3 \epsilon_3 \delta_{I,3}\ , \quad B^I_{2,1} = \rho_I \frac{\partial \beta_I}{\partial \xi_2} + \frac{1}{2}\rho_4 \epsilon_4 \delta_{I,4}\ , \quad C^I_{i,1} = \rho_I \frac{\partial \beta_I}{\partial \bar{\xi}_i}\,, \end{aligned} \tag{7.29}$$

where

$$\epsilon_I \equiv 8\beta_I^2 - 6\gamma_I\,. \tag{7.30}$$

The coefficients β_I and γ_I can be calculated from the expression of the quadratic differential (2.4) and (2.12). First we expand $\varphi = \phi(z)(dz)^2$ around the puncture z_I

$$\phi(z) = -\frac{1}{(z - z_I)^2} + \frac{r^I_{-1}}{(z - z_I)} + r^I_0 + \mathcal{O}(z)\,, \tag{7.31}$$

and knowing that in the local coordinates φ takes the canonical form

$$\varphi = -\frac{1}{w_I^2}(dw_I)^2\,, \tag{7.32}$$

we find the relations

$$\beta_I = \frac{1}{2} r^I_{-1} \quad , \quad \gamma_I = \frac{1}{16}\left(7(r^I_{-1})^2 + 4(r^I_0)^2\right)\,. \tag{7.33}$$

And after expanding $\phi(z)$ to obtain r^I_{-1} and r^I_0, we find

$$\begin{aligned} \beta_1 &= \frac{a_1 - \xi_1^2 - \xi_2^2}{2\xi_1\xi_2} \\ \beta_2 &= -\frac{a_1 + a_2 + 2\xi_1 - \xi_1^2 + 2\xi_2 - \xi_2^2}{2(\xi_1 - 1)(\xi_2 - 1)} \\ \beta_3 &= \frac{a_1 - 2\xi_1^2 - \xi_2^2 + \xi_1(3 + a_2 + 2\xi_2)}{2\xi_1(\xi_1 - 1)(\xi_2 - \xi_1)} \\ \beta_4 &= \frac{a_1 - \xi_1^2 + 2\xi_1\xi_2 + \xi_2(3 + a_2 - 2\xi_2)}{2\xi_2(\xi_2 - 1)(\xi_1 - \xi_2)} \\ \beta_5 &= -\frac{1}{2}\left(2 + a_2 + \xi_1 + \xi_2\right)\,, \end{aligned} \tag{7.34}$$

and for $\epsilon_I = 8\beta_I^2 - 6\gamma_I$, we find

$$\begin{aligned}
\epsilon_1 &= \frac{-5(u-a_1)^2 + 12\left((\xi_1^3+\xi_2^2)(1+\xi_2) - a_1(s+t) + \xi_1^2(1-\xi_2+\xi_2^2) + t(-3-a_2-\xi_2+\xi_2^2)\right)}{8t^2} \\
\epsilon_2 &= \frac{-5(u-2s-a_1-a_2)^2 - 12\left(5s-7u+2w+t(4s-5-u-t) - a_2(s-2) - a_1(2s-t-3)\right)}{8(t-s+1)^2} \\
\epsilon_3 &= \frac{1}{8(\xi_1(\xi_1-\xi_2)(\xi_1-1))^2}\left(4\xi_1^3(10\xi_1 - 15 - a_2 - 14\xi_2) - a_1(5a_1 + 16\xi_1^2 + 2\xi_1(3+5a_2-2\xi_2)\right. \\
&\qquad +2(6-5\xi_2)\xi_2) + \xi_2^2(12(1+\xi_2) - 5\xi_2^2) - 2t(12 + 9\xi_2 - 5a_2\xi_2 + 2\xi_2^2) \\
&\qquad \left.+\xi_1^2(15 - 18a_2 - 5a_2^2 + 24\xi_2 - 8a_2\xi_2 + 44\xi_2^2)\right) \\
\epsilon_4 &= \frac{-1}{8(\xi_2(\xi_1-\xi_2)(\xi_2-1))^2}\left(-a_1(-5a_1 + 10\xi_1^2 - 12\xi_1 + 4t + 2(-5a_2 - 3 - 8\xi_2)\xi_2)\right. \\
&\qquad +2\xi_1^2(-6 + (9-5a_2)\xi_2 - 22\xi_2^2) + 8t(3 - (3-a_2)\xi_2 + 7\xi_2^2) \\
&\qquad \left.-\xi_2^2(15 - 18a_2 - 5a_2^2 - 60\xi_2 - 4a_2\xi_2 + 40\xi_2^2) + \xi_1^3(5\xi_1 - 12 + 4\xi_2)\right) \\
\epsilon_5 &= \frac{1}{8}\left(16 + 12a_1 + 4s + 7u + 2t + a_2(-5a_2 - 8 + 2s)\right) ,
\end{aligned} \tag{7.35}$$

where we have defined

$$s \equiv \xi_1 + \xi_2 \ , \quad t \equiv \xi_1\xi_2 \ , \quad u \equiv \xi_1^2 + \xi_2^2 \ , \quad w \equiv \xi_1^3 + \xi_2^3 \, . \tag{7.36}$$

We will also need to compute a few correlators. To see which ones, it is best to start expanding the antighost insertions. It is easily seen from the expression for the dilaton and the fact that only the correlators with ghost number $(3,\bar{3})$ do not vanish, that we need either three b's and one $\bar{b}$, or one b and three $\bar{b}$'s; and as already mentioned we only need antighost oscillators with indices -1 or 1. Let us expand $(\mathcal{B}\mathcal{B}^\star)_1 (\mathcal{B}\mathcal{B}^\star)_2$ in the following way: we take all terms in the first factor that have either two b's or two $\bar{b}$'s and mixed terms in the second factor. The rest of the expression, with mixed terms in the first factor, can be found simply by changing some indices

$$\begin{aligned}
&(\mathcal{B}\mathcal{B}^\star)_1 (\mathcal{B}\mathcal{B}^\star)_2 = \\
&= \left(B^3_{1,-1} b^{(3)}_{-1} \sum_{I=1}^{5} C^I_{1,1} b^{(I)}_1 - \overline{B^3_{1,-1}} \bar{b}^{(3)}_{-1} \sum_{I=1}^{5} \overline{C^I_{1,1}} \bar{b}^{(I)}_1 + \sum_{I\neq J} B^I_{1,1} C^J_{1,1} b^{(I)}_1 b^{(J)}_1 - \sum_{I\neq J} \overline{B^I_{1,1} C^J_{1,1}} \bar{b}^{(I)}_1 \bar{b}^{(J)}_1 \right) \\
&\times \left(B^4_{2,-1} b^{(4)}_{-1} \sum_{I\neq 4} \overline{B^I_{2,1}} \bar{b}^{(I)}_1 - \overline{B^4_{2,-1}} \bar{b}^{(4)}_{-1} \sum_{I\neq 4} B^I_{2,1} b^{(I)}_1 + \sum_{I\neq J} M^{IJ}_2 b^{(I)}_1 \bar{b}^{(J)}_1 \right) + \left(1 \leftrightarrow 2 \ , \ ^3 \leftrightarrow ^4\right) \ ,
\end{aligned} \tag{7.37}$$

where

$$M^{IJ}_i \equiv B^I_{i,1} \overline{B^J_{i,1}} - C^I_{i,1} \overline{C^J_{i,1}} \, , \tag{7.38}$$

and the last term is obtained by changing as indicated the left subscripts of B and C, the subscript of M, and all superscripts. Noting that

$$b_{-1}|D\rangle = c_{-1}|0\rangle \ , \quad b_1|D\rangle = -c_1|0\rangle \ , \quad \bar{b}_{-1}|D\rangle = -\bar{c}_{-1}|0\rangle \ , \quad \bar{b}_1|D\rangle = \bar{c}_1|0\rangle \, , \tag{7.39}$$

we see from (7.37), that we need the following open correlators

$$\begin{aligned} &A_{IJ} \equiv \langle (c_{-1}c_1)^{(I)}, c_{-1}^{(J)} \rangle_o \ , \quad B_{IJ} \equiv \langle (c_{-1}c_1)^{(I)}, c_1^{(J)} \rangle_o \\ &C_{IJK} \equiv \langle c_1^{(I)}, c_1^{(J)}, c_1^{(K)} \rangle_o \ , \quad D_{IJK} \equiv \langle c_{-1}^{(I)}, c_1^{(J)}, c_1^{(K)} \rangle_o \ , \quad E_{IJK} \equiv \langle c_{-1}^{(I)}, c_{-1}^{(J)}, c_1^{(K)} \rangle_o \, . \end{aligned} \tag{7.40}$$

The conventions for the closed correlators are as in [11]

$$\langle c(z_1)c(z_2)c(z_3)\bar{c}(\bar{w}_1)\bar{c}(\bar{w}_2)\bar{c}(\bar{w}_3)\rangle = -2\langle c(z_1)c(z_2)c(z_3)\rangle_o \, \langle \bar{c}(\bar{w}_1)\bar{c}(\bar{w}_2)\bar{c}(\bar{w}_3)\rangle_o \, , \tag{7.41}$$

and the open correlator is

$$\langle c(z_1)c(z_2)c(z_3)\rangle_o = (z_1 - z_2)\,(z_1 - z_3)\,(z_2 - z_3) \, . \tag{7.42}$$

A_{IJ} and B_{IJ} were already calculated in [11]. For the other correlators, we can use either the conformal transformation of the operator $\frac{1}{2}\partial^2 c(z)$ corresponding to c_{-1} (as in [11]), or conservation laws as in [15]. We find when $I, J, K \neq 5$

$$\begin{aligned} A_{IJ} &= \rho_J \left(\beta_J - \beta_I - 2\beta_I\beta_J z_{IJ} + \frac{1}{2}\epsilon_J z_{IJ}(1 - \beta_I z_{IJ}) \right) \\ B_{IJ} &= \frac{1}{\rho_J} z_{IJ}(1 - \beta_I z_{IJ}) \\ C_{IJK} &= \frac{1}{\rho_I\rho_J\rho_K} z_{IJ}z_{IK}z_{JK} \\ D_{IJK} &= \frac{\rho_I}{\rho_J\rho_K} \left(z_{JK} - \beta_I(z_{IK} + z_{IJ})z_{JK} + \frac{1}{2}\epsilon_I z_{IJ}z_{JK}z_{IK} \right) \\ E_{IJK} &= \frac{\rho_I\rho_J}{\rho_K} \Big(\beta_I - \beta_J + \beta_I\beta_J(z_{IJ} + z_{IK} - z_{JK}) + \frac{1}{2}\epsilon_J z_{JK} - \frac{1}{2}\beta_I\epsilon_J(z_{IJ} + z_{IK})z_{JK} + \\ &\qquad + \frac{1}{2}\epsilon_I \left(-z_{IK} + \beta_J z_{IK}(z_{JK} - z_{IJ}) + \frac{1}{2}\epsilon_J z_{IJ}z_{IK}z_{JK} \right) \Big) \quad , \quad I, J, K \neq 5 \, . \end{aligned} \tag{7.43}$$

The cases when one oscillator is at infinity must be treated separately. Since $B^5_{i,-1}$ and $C^5_{i,-1}$ are zero, only c_1 can be at infinity. We therefore need

$$\begin{aligned} A_{5J} &= \rho_J \left(\frac{1}{2}\epsilon_J(\beta_5 + z_J) - \beta_J \right) \\ B_{I5} &= \frac{\beta_I}{\rho_5} \quad , \quad B_{5J} = \frac{1}{\rho_J}(z_J + \beta_5) \\ C_{IJ5} &= \frac{z_{JI}}{\rho_I\rho_J\rho_5} \\ D_{IJ5} &= \frac{\rho_I}{\rho_J\rho_5} \left(\beta_I - \frac{1}{2}\epsilon_I z_{IJ} \right) \\ E_{IJ5} &= \frac{\rho_I\rho_J}{\rho_5} \left(\frac{1}{2}\beta_I\epsilon_J - \frac{1}{2}\epsilon_I\beta_J - \frac{1}{4}\epsilon_I\epsilon_J z_{IJ} \right) , \end{aligned} \tag{7.44}$$

and we note that C_{IJK} is totally antisymmetric, D_{IJK} is antisymmetric in J and K, and E_{IJK} is antisymmetric in I and J.

We can now write the integrand of (7.25) with five dilatons from (7.37) and the definitions (7.40).

$$
\begin{aligned}
&\langle\Sigma|\left(\mathcal{B}\mathcal{B}^\star\right)_1\left(\mathcal{B}\mathcal{B}^\star\right)_2|D\rangle|D\rangle|D\rangle|D\rangle|D\rangle = \\
&= 4\,\mathrm{Re}\Bigg\{\frac{1}{\rho_3\rho_4}\sum_{3\neq4\neq I\neq J\neq K}\Big\{\overline{A_{k3}}\left(D_{4IJ}C^I_{2,1}B^J_{1,1}-B_{IJ}C^4_{2,1}B^J_{1,1}+B_{JI}C^I_{2,1}B^4_{1,1}\right) \\
&\qquad +\overline{A_{K4}}\left(D_{3IJ}C^I_{1,1}B^J_{2,1}-B_{IJ}C^3_{1,1}B^J_{2,1}+B_{JI}C^I_{1,1}B^3_{2,1}\right) \\
&+\overline{B_{KJ}}\left(-E_{34I}\left(C^I_{1,1}\overline{B^J_{2,1}}-C^I_{2,1}\overline{B^J_{1,1}}\right)+\overline{B^J_{2,1}}\left(A_{I3}C^4_{1,1}-A_{I4}C^3_{1,1}\right)+\overline{B^J_{1,1}}\left(A_{I4}C^3_{2,1}-A_{I3}C^4_{2,1}\right)\right)\Big\} \\
&\quad+\frac{1}{\rho_3}\sum_{3\neq I\neq J\neq K\neq L}\Big\{\overline{B_{LK}}\Big(-D_{3IJ}C^I_{1,1}M^{JK}_2+B_{IJ}C^3_{1,1}M^{JK}_2-B_{JI}C^I_{1,1}M^{3K}_2 \\
&\qquad +\overline{B^K_{1,1}}\left(-D_{3IJ}B^I_{2,1}C^J_{2,1}+B_{IJ}B^3_{2,1}C^J_{2,1}-B_{JI}B^I_{2,1}C^3_{2,1}\right)\Big)-C_{IJK}\overline{A_{L3}}B^I_{2,1}C^J_{2,1}B^K_{1,1}\Big\} \\
&\quad+\frac{1}{\rho_4}\sum_{4\neq I\neq J\neq K\neq L}\Big\{\overline{B_{LK}}\left(-D_{4IJ}C^I_{2,1}M^{JK}_1+B_{IJ}C^4_{2,1}M^{JK}_1-B_{JI}C^I_{2,1}M^{4K}_1\right. \\
&\qquad \left.+\overline{B^K_{2,1}}\left(-D_{4IJ}B^I_{1,1}C^J_{1,1}+B_{IJ}B^4_{1,1}C^J_{1,1}-B_{JI}B^I_{1,1}C^4_{1,1}\right)\right)-C_{IJK}\overline{A_{L4}}B^I_{1,1}C^J_{1,1}B^K_{2,1}\Big\} \\
&\quad+\sum_{I\neq J\neq K\neq L\neq T}C_{IJK}\overline{B_{TL}}\left(B^I_{1,1}C^J_{1,1}M^{KL}_2+B^I_{2,1}C^J_{2,1}M^{KL}_1\right)\Bigg\}\,. \qquad (7.45)
\end{aligned}
$$

With (7.29), (7.34), (7.35), (7.43) and (7.44), this expression can be expressed in terms of ξ_i, a_i, $\partial a_i/\partial\xi_j$, $\partial a_i/\partial\bar{\xi_j}$ and ρ_I, and we can therefore integrate it numerically over the reduced moduli space of five-punctured spheres. Since we have five times the same state, the result is simply 120 times the integral on $\mathcal{A}_5$, thus

$$
\kappa^2 V_{d^5} = \frac{1}{5!}\{D,D,D,D,D\} = \frac{1}{\pi^2}\int_{\mathcal{A}_5} dx_1\wedge dy_1\wedge dx_2\wedge dy_2\langle\Sigma|\left(\mathcal{B}\mathcal{B}^\star\right)_1\left(\mathcal{B}\mathcal{B}^\star\right)_2|D\rangle|D\rangle|D\rangle|D\rangle|D\rangle\,. \qquad (7.46)
$$

We do the integration as in Section 6, on three different grids. The results are shown in Table 3. They are compatible within their error bounds, and we take again the result from the finest grid

(N,h,s)	$(30,0.1,0.1)$	$(70,0.05,0.05)$	$(70,0.05,0.04)$
$\kappa^2 V_{d^5}(2h)$	-0.30666 ± 0.0093	-0.30768 ± 0.0023	-0.30759 ± 0.0016
$\kappa^2 V_{d^5}(h)$	-0.30343 ± 0.0093	-0.30666 ± 0.0023	-0.30660 ± 0.0016
$\kappa^2 V_{d^5}$	-0.3024 ± 0.0093	-0.3063 ± 0.0023	-0.3063 ± 0.0016

Table 3: The results of the integration (7.46) and its uncertainty on three different grids.

as final answer

$$
\boxed{\kappa^2 V_{d^5} = -0.3063\pm0.0016}\,. \qquad (7.47)
$$

We see that (7.18) and (7.47) cancel each other with a precision of about 0.1%, well within the error bound of 0.5% on the contact term (7.47). This is solid evidence that our computations are reliable.

8 Conclusions and prospects

In the light of the verification successfully made in Section 7, that the effective potential of the dilaton vanishes at order five, we can claim that the techniques described in this paper work well, that the reduced moduli space is understood and described right, and that our implementation of the algorithm gives reliable results. In particular we trust the value (6.12) obtained for the contact term of five tachyons. It is also a good check of the consistency of CSFT itself.

We are able to estimate the uncertainty made in the computation of terms. However we want to mention here that we have been quite conservative in this estimation. In particular the errors on the fits were treated as systematic instead of independent. This is only half right because we expect interpolations made from different samples to be more or less independent, although two interpolations at two nearby points using the same sample will be completely dependent. The overestimation of the error seems confirmed by the values in Tables 1 and 3. However one should be careful in this respect because, as we already mentioned, we don't think that the errors made on different grids are independent either. So unless we find a better way of estimating the error, we will stick to our conservative estimation. Any way, we emphasize that the errors on any given term will probably be no more than 0.5%, the error we find for the five-dilaton term (which is calculated from a very long expression). And this precision is probably enough to do level truncation.

The effect of the five-tachyon term (6.12) on the stable vacuum is studied in [15]. However this term of level zero isn't enough to draw any conclusion. For this, it will be necessary to compute other terms at higher level. At level two there is only one term, namely four tachyons and one dilaton V_{t^4d}. At level four we'll have five terms, $V_{t^3d^2}$ and $V_{t^4\psi_i}$ where $|\Psi_i\rangle$, $i = 3, \ldots, 6$, are the four scalar fields at level four. The main difficulty in computing these terms will be that when we have different external states, the integrations on the 120 pieces of reduced moduli space won't be all equal, and it will require some (straightforward but lengthy) work to express them as one integral over $\mathcal{A}_5$; the extreme case being when we have five different states, we will have 60 different integrals (complex conjugation is always trivial and divides the number of integrations by two). But the computation of interactions to level four is certainly not that bad. By automatizing the computation of oscillator algebra and correlators, as in [15], it might be possible to compute higher levels as well.

At last, it would be useful to make our numerical data available, so that readers can use it to make their own computations of quintic terms. Ideally we would like to create fits of the boundaries of the moduli space and the parameters of the quadratic differentials a_1 and a_2 and the mapping radii, that could hold in a paper and be entered in a computer in a reasonable amount of time. This is under study, but we are a bit pessimistic given the dimensionality and rather complicated shape of the reduced moduli space (our data describing its boundary is about 600 megabytes large).

Acknowledgments

I am indebted to Barton Zwiebach for many useful discussions. This work has been funded by an "EC" fellowship within the framework of the "Marie Curie Research Training Network" Programme, Contract no. MRTN-CT-2004-503369.

References

[1] B. Zwiebach, "Closed string field theory: Quantum action and the B-V master equation," Nucl. Phys. B **390**, 33 (1993) [arXiv:hep-th/9206084];

[2] T. Kugo, H. Kunitomo and K. Suehiro, "Nonpolynomial Closed String Field Theory," Phys. Lett. B **226**, 48 (1989); T. Kugo and K. Suehiro, "Nonpolynomial Closed String Field Theory: Action And Its Gauge Invariance," Nucl. Phys. B **337**, 434 (1990); H. Sonoda and B. Zwiebach, "Covariant Closed String Theory Cannot Be Cubic," Nucl. Phys. B **336**, 185 (1990); B. Zwiebach, "Quantum Closed Strings From Minimal Area," Mod. Phys. Lett. A **5**, 2753 (1990); M. Kaku, "Geometric Derivation Of String Field Theory From First Principles: Closed Strings And Modular Invariance," Phys. Rev. D **38**, 3052 (1988).

[3] M. Saadi and B. Zwiebach, "Closed String Field Theory From Polyhedra," Annals Phys. **192**, 213 (1989);

[4] B. Zwiebach, "Consistency Of Closed String Polyhedra From Minimal Area," Phys. Lett. B **241**, 343 (1990); B. Zwiebach, "How Covariant Closed String Theory Solves A Minimal Area Problem," Commun. Math. Phys. **136**, 83 (1991).

[5] E. Witten, "Noncommutative Geometry And String Field Theory," Nucl. Phys. B **268** (1986) 253.

[6] V. A. Kostelecky and S. Samuel, "Collective physics in the closed bosonic string," Phys. Rev. D **42** (1990) 1289.

[7] N. Moeller, "Closed bosonic string field theory at quartic order," JHEP **0411** (2004) 018 [arXiv:hep-th/0408067].

[8] K. Strebel, "Quadratic Differentials," Springer Verlag, 1984.

[9] A. Belopolsky and B. Zwiebach, "Off-shell closed string amplitudes: Towards a computation of the tachyon potential," Nucl. Phys. B **442**, 494 (1995) [arXiv:hep-th/9409015].

[10] H. Yang and B. Zwiebach, "Testing closed string field theory with marginal fields," JHEP **0506**, 038 (2005) [arXiv:hep-th/0501142].

[11] H. Yang and B. Zwiebach, "Dilaton deformations in closed string field theory," JHEP **0505**, 032 (2005) [arXiv:hep-th/0502161].

[12] H. Yang and B. Zwiebach, "A closed string tachyon vacuum?," JHEP **0509**, 054 (2005) [arXiv:hep-th/0506077].

[13] H. Yang and B. Zwiebach, "Rolling closed string tachyons and the big crunch," JHEP **0508**, 046 (2005) [arXiv:hep-th/0506076].

[14] A. Belopolsky, "Effective Tachyonic potential in closed string field theory," Nucl. Phys. B **448**, 245 (1995) [arXiv:hep-th/9412106].

[15] N. Moeller and H. Yang, "The nonperturbative closed string tachyon vacuum to high level," arXiv:hep-th/0609208.

[16] N. Moeller, Work in progress.

[17] A. Ralston and P. Rabinowitz, "A First Course in Numerical Analysis," McGraw-Hill, 1978, Second Edition.

[18] W. H. Press, S. A. Teukolsky, W. T. Vetterling, B. P. Flannery, "Numerical Recipes in C++," Cambridge University Press, Second Edition.